Barbara Angerer, BSc

Requirements for future satellite gravity missions to detect meso-scale ocean variability

MASTER'S THESIS

to achieve the university degree of

Diplom-Ingenieurin

Master's degree programme: Geomatics Science

submitted to

Graz University of Technology

Supervisor

Univ.-Prof. Dr.-Ing. Torsten Mayer-Gürr

Institut für Geodäsie

Graz, September 2015

AFFIDAVIT

I declare that I have authored this thesis independently, that I have not used other than the declared sources/resources, and that I have explicitly indicated all material which has been quoted either literally or by content from the sources used. The text document uploaded to TUGRAZonline is identical to the present master‘s thesis dissertation.

Date

Signature

Acknowledgement

At this point I would like to grab the chance to thank all the people who supported me in writing this master thesis. First of all I would like to express my gratitude to my parents for their everlasting support during my studies and in special during the last year, both in financial and mental respect. Thank you for making it possible for me to study whatever I desired to and for always believing in me.

Furthermore I would particularly like to thank my supervisor Univ.-Prof. Dr.-Ing. Torsten Mayer-Gürr for spending so much of his time on answering all my questions that arose throughout the work on this thesis. The countless discussions were a great support and helped me to find the right direction.

Very special thanks also to my boyfriend for his understanding during this stressful time and for always finding motivating words for me. In addition, I would like to thank my friends, who gave me the much needed balance and diversion during the past months. Finally I owe thanks to Barbara Falkner for her effort in proofreading this thesis.

Thank you!

Abstract

The satellite gravity mission GRACE provides important information on the earth‘s time-variable gravity field. However, the detection of time-variable signals is strongly limited by the spatial and temporal resolution of GRACE. Meso-scale ocean processes with an average spatial extent of 100 km have therefore remained hidden for GRACE so far. The exploration of meso-scale processes is gaining significance because of their possible impact on our climate, hence future satellite missions also aim to detect these meso-scale variations in the earth´s gravity field. To determine the current possibilities of GRACE concerning the detection of such processes and to give a statement on the required improvement in accuracy, an analysis using the ITSG-Grace2014 gravity field solution and the ocean component of the updated ESA ESM has been conducted. The difficulty in extracting the oceanic signal from the integral GRACE signal is demonstrated by means of the evaluation of the eustatic sea-level rise. For the investigations regarding the meso-scale variations, ocean bottom pressure anomalies in two representative observation areas (Argentine Basin and Cape Basin) are analyzed. As the investigations showed, a globally valid statement about the improvement in accuracy can not be given because of the various GRACE error sources as well as the regional characteristics of the meso-scale ocean processes.

Kurzfassung

Die Schwerefeldmission GRACE liefert wichtige Informationen über das Schwerefeld der Erde. Allerdings ist die Detektion von zeit-variablen Signalen stark durch die räumliche und zeitliche Auflösung von GRACE limitiert. Meso-skalige Ozeanprozesse mit einer durschnittlichen räumlichen Auflösung von 100 km blieben dadurch von GRACE bislang unentedeckt. Die Erforschung der meso-skaligen Ozeanprozesse gewinnt aber immer mehr an Bedeutung da ihnen ein Einfluss auf unser Klima nachgesagt wird, weswegen sich auch zukünftige Satellitenmissionen mit der Detektion von meso-skaligen Veränderungen beschäftigen. Um die jetzigen Möglichkeiten von GRACE bezüglich der Detektion solcher Prozesse festzustellen und eine Abschätzung für die Genauigkeitsverbesserung von zukünftigen Schwerefeldmissionen zu geben, wurde eine Analyse an Hand der ITSG-Grace2014 Schwerefeldlösung und der Ozeankomponente des aktualisierten ESA ESM durchgeführt. Die Schwierigkeit der Extraktion des Ozeansignals aus dem integralen GRACE Signal wird mittels der Berechnung des eustatischen Meeresspiegels herausgearbeitet. Für die Untersuchungen bezüglich der meso-skaligen Variabilitäten werden Ozeanbodendruckanomalien in zwei repräsentativen Beobachtungsgebieten (Argentinisches Becken und Agulhas Becken) analysiert. Eine global gültige Abschätzung für die nötige Verbesserung in der Genauigkeit kann auf Grund der unterschiedlichen Fehlerquellen von GRACE, als auch des regionalen Charakters der meso-skaligen Ozeanprozesse nicht gegeben werden.

Contents

1 Introduction

The curiosity of the human beings on the planet that shares our habitat has already been long lasting. Consequently, the exploration of the earth has always been in the focus of a huge variety of scientific researches. With the beginning of the satellite era in the second stage of the previous century, an innovative technique in gathering new information and insights on our planet was found. Various satellite missions have contributed greatly to recent scientific findings concerning geophysical processes on and in the earth. Much of the knowledge about the earth´s gravity field is owed to the satellite gravity mission GRACE (*Gravity Recovery and Climate Experiment*), which supplies not only information on the static but also on the time variable part of the gravity field.

Although a good deal is already known about the processes going on in ocean, atmosphere and inside the earth, by far not all of the complex processes in the different subsystems, their interactions as well as their impact on our climate have been clarified completely. One example is the occurrence of so-called meso-scale ocean eddies, which are suspected to have a great impact on our future climate. Eddies in the region around the Cape Agulhas are influencing the Gulf Stream, which is known to be determining the climate in the northern hemisphere. This is one good reason why the interest in understanding the complexity of meso-scale processes is increasing. Especially future satellite missions might be able to contribute important information on those processes.

The aim of this thesis is to demonstrate the current possibility of GRACE for the detection of such meso-scale ocean variability by means of a comparison with simulated ocean data from the updated ESA ESM (*ESA Earth System Model*). Furthermore a statement on the required improvement in accuracy for future satellite gravity missions to adequately resolve meso-scale eddies shall be given.

The thesis is structured as follows. Chapter 2 focuses on the GRACE mission, in particular on the available gravity field solutions and the mandatory post-processing steps. Moreover some analysis methods are explained in more detail. In chapter 3 the structure and contents of the updated ESA ESM will be illustrated with a special focus on the oceanic component (*O component*). In chapter 4 the eustatic sea-level rise is evaluated, highlighting the differences that have to be taken into account when working with model and gravity field data. Chapter 5 will give an insight into the meso-scale ocean processes, dealing with their emergence as well as their properties and distinct occurrences. In the subsequent chapter 6 ocean bottom pressure (*OBP*) signals are analyzed and compared using different methods. From this a conclusion on the detectability of meso-scale variability of the current GRACE mission is drawn as well as a statement about future requirements is given. The last chapter contains an outlook on future satellite gravity missions and their efforts.

2 GRACE

The GRACE (*Gravity Recovery and Climate Experiment*) mission, consisting of a tandem satellite pair flying at an altitude of 450 km, is a joint project of the NASA (*National Aeronautics and Space Administration*) and the DLR (*Deutsches Zentrum für Luft- und Raumfahrt*). The mission makes use of a different measurement principle (SST-ll, *Satellite-to-Satellite Tracking in low-low configuration*) compared to the forerunner mission CHAMP (*Challenging Mini Satellite Payload*) and supplies high-precision information on the static earth´s gravity field as well as on the time variable field. On account of the innovative measuring principle, the time variable gravity field can be determined at a degree of accuracy never achieved before by any satellite gravity mission. The GRACE twin satellites, started in 2002, are still providing data at this moment of time (06/2015) and are thus greatly exceeding the planned mission duration of five years. Due to the capital success of GRACE a succession mission is planned to be started in 2017. The main goal of GRACE-FO (*GRACE Follow On*) is the continuation of the current measurements to receive long-term time series of the time variable gravity field. Nevertheless GRACE-FO shall be able to deliver even more precise models of the static and time variable gravity field than the GRACE-1 mission.

The following sections shall give an overview of the theoretical background of the earth's gravity field, giving insight into the mathematical definition as well as the geophysical signals observed by GRACE. Furthermore the mandatory post-processing steps when working with GRACE data are presented. The final section demonstrates the used analysis methods.

2.1 GRACE gravity field solutions

Basically a great variation of different GRACE gravity field solutions is available, as certain institutes working in the research sector of satellite geodesy, are processing their own solution. The official data centers for GRACE gravity field solutions are the CSR (*Texas Center for Space Research*), the GFZ (*GeoForschungsZentrum Potsdam*) and the JPL (*Jet Propulsion Laboratory*). For the investigations during this thesis the gravity field solution ITSG-Grace2014 (Mayer-Gürr et al., 2014) from the *Institute of Geodesy* in Graz has been used. The solution is available from February 2003 until December 2013, missing some months due to erroneous GRACE data. The monthly solutions are obtainable in form of Stokes coefficients up to degree 60, 90 and 120, the static solution until degree 200.

Beside the monthly solutions also the daily ITSG solutions, determined through kalman filtering, have been used for the examinations. Those are available for the same time span, but only until degree 40.

2.1.1 Spherical harmonics

The mathematical definition of the earth´s gravity field has its origin in Newton's law of universal gravity. Newton stated, that two bodies attract each other with a force F which is directed along the connection line of these bodies. This force is called the gravitational force F and its strength is directly proportional to the product of both masses and inversely proportional to the square of their intermediate distance

$$\overrightarrow{F} = -G \cdot \frac{m_1 m_2}{r^2} \cdot \frac{\overrightarrow{r}}{r}. \tag{2.1}$$

Starting from this, the gravitational potential of a point mass can be expressed

$$V = \frac{Gm}{r}. \tag{2.2}$$

If not a single point, but an extensive body, such as the earth is observed, the density as well as the volume of the body is needed. This leads to the following depiction of the gravitational potential

$$V(r) = G \iiint_{\Omega} \frac{\rho_Q(r_Q)}{\|r - r_Q\|} d\Omega. \tag{2.3}$$

This equation demonstrates the relation between the mass distribution of a body (Ω) and the mass indicated gravitational potential V at the receiving point r. As the density of the earth is not sufficiently known, the gravitational potential at one distinct point can not be solved by this equation. However, for the exterior of the sphere a converging series expansion of V as a special solution of the Laplace equation can be successfully done.

This yields the common mathematical description of the gravitational potential in terms of a series expansion in spherical harmonics (Heiskanen and Moritz, 1967). The gravity potential for the exterior of the sphere expressed in spherical harmonics is

$$V(r, \theta, \lambda) = \frac{GM}{R} \sum_{n=0}^{\infty} \left(\frac{R}{r}\right)^{(n+1)} \sum_{m=0}^{n} \overline{P}_{nm}(\cos\theta)[\overline{c}_{nm} \cos m\lambda + \overline{s}_{nm} \sin m\lambda]. \tag{2.4}$$

$\overline{P}_{nm}(cos\theta)$ defines the fully normalized Legendre Functions (of degree n and order m), $\overline{c}_{nm}$ and $\overline{s}_{nm}$ are the fully normalized spherical harmonic coefficients, also called Stokes coefficients. The position vector r is given in polar coordinates, with λ being the longitude, θ the polar distance and r the radial component. GM is the geocentric gravitational constant ($3.986004418 \cdot 10^{14} \frac{m^3}{s^2}$) and R (6378.1366 km) the mean earth radius.

The fully normalized Stokes coefficients are determined through the density distribution $\rho_Q(r_Q)$ in all source points $r_Q = (r, \lambda, \theta)_Q$ of the attracting body

$$\left.\begin{matrix} c_{nm} \\ s_{nm} \end{matrix}\right\} = \frac{1}{2n+1} \cdot \frac{1}{M} \iiint_{\Omega} \left(\frac{r_Q}{R}\right)^n \rho_Q(r_Q, \lambda_Q, \theta_Q) \left\{\begin{matrix} C_{nm}(\lambda_Q, \theta_Q) \\ S_{nm}(\lambda_Q, \theta_Q) \end{matrix}\right\} d\Omega. \tag{2.5}$$

Because the density distribution of the earth is not constant due to ongoing geophysical processes, a time-dependency of the Stokes coefficients has to be regarded

$$\left.\begin{matrix} c_{nm}(t) \\ s_{nm}(t) \end{matrix}\right\} = \frac{1}{2n+1} \cdot \frac{1}{M} \iiint_{\Omega} \left(\frac{r_Q}{R}\right)^n \rho_Q(t, r_Q, \lambda_Q, \theta_Q) \left\{\begin{matrix} C_{nm}(\lambda_Q, \theta_Q) \\ S_{nm}(\lambda_Q, \theta_Q) \end{matrix}\right\} d\Omega. \tag{2.6}$$

Considering the time-variable Stokes coefficients, one can define a time-dependent gravitational potential

$$V(t, r, \lambda, \theta) = \frac{GM}{R} \sum_{n=0}^{\infty} \left(\frac{R}{r}\right)^{(n+1)} \sum_{m=0}^{n} [c_{nm}(t) C_{nm}(\lambda, \theta) + s_{nm}(t) S_{nm}(\lambda, \theta)]. \tag{2.7}$$

If a certain mass distribution is given, the gravitational potential can be determined explicitly. The inverse way however is unambiguous, as there are several different mass distributions that generate the exact same gravitational potential in the exterior. The solution of this problem is the assumption of a thin layer (Bryan et al., 1998) in which the mass distributions occur. This assumption is valid as the dimension of ocean and atmosphere together is very small compared to the total mean earth radius. This yields the appropriate coefficients of the gravitational potential of the exterior:

$$\left.\begin{matrix} c_{nm}(t) \\ s_{nm}(t) \end{matrix}\right\} = \frac{1}{2n+1} \cdot \frac{M}{4\pi R^2} \iint_{\Phi} \sigma(t, r_\Phi) \left\{\begin{matrix} C_{nm}(r_\Phi) \\ S_{nm}(r_\Phi) \end{matrix}\right\} d\Phi \tag{2.8}$$

with the surface density $\sigma(t, r_\Phi)$ that can again be expanded in a series of spherical harmonics

$$\sigma(t, r_\Phi) = \sum_{n=0}^{\infty} \sum_{m=0}^{n} a_{nm}(t) C_{nm}(\lambda, \theta) + b_{nm}(t) S_{nm}(\lambda, \theta). \tag{2.9}$$

For the determination of the mass coefficients out of potential coefficients, such as observed by GRACE,

$$\left.\begin{matrix} a_{nm}(t) \\ b_{nm}(t) \end{matrix}\right\} = (2n+1) \frac{M}{4\pi R^2} \left\{\begin{matrix} c_{nm}(t) \\ s_{nm}(t) \end{matrix}\right\} \tag{2.10}$$

has to be applied. Further detailed information on the mathematical description of the earth´s gravity field can be found in (Heiskanen and Moritz, 1967) and (Kurtenbach, 2011).

2.1.2 Signals

The variations in the earth´s gravity field are generated due to mass redistribution in the different layers of the earth. With the help of the GRACE mission geophysical signals such as the sea-level rise, seasonal variation of the water budget of rivers and river basins as well as the melting of continental ice masses can be observed. These superimposing effects form the earth's time-variable gravity field. For the detailed consideration of one distinct signal the greatest challenge is to separate the mutually interfering signals. To succeed in this, an accurate knowledge of the occurring signals is unavoidable. Hence the following section will list the most important mass variations on and in the earth.

Tides

The gravitational forces of sun and moon are causing effects on the earth that are known through the term of tides. Because of the tidal forces enormous water masses are displaced periodically (daily and sub daily) on the earth´s surface, which consequently leads to a change in the gravity field. Beside the effect on water masses, the tidal forces do also act on the solid earth (solid earth tides). The tide induced variations are the by far greatest time- variable signal observed by GRACE.

Atmosphere, ocean and continental signal

Mass transports in the atmosphere can be caused due to changes in humidity, pressure, temperature etc. Ocean currents driven by wind, but also through temperature and salinity changes are also leaving their footprints in the time-variable gravity field. Changes in the ground-water level, soil moisture as well as the runoff of big rivers belong to the continental hydrological signal. The greatest contribution to this signal is the melting of the continental ice shields, such as in Greenland. The variations in atmosphere, ocean and the continental hydrology are roughly in the same magnitude.

Solid earth

The previously described time variable signals mainly concern short-periodic variations, having daily to yearly periods. But also events that occur suddenly and irregularly, e.g. earthquakes or volcanic eruptions do have an effect on the gravity field and yield locally high variations. Beside these spontaneous happenings also long-term variations of the solid earth exist, the so called post glacial rebound (PGR) or glacial isostatic adjustment (GIA) (see section 4.3.1). Also processes in the core and the mantle belong to the long-term variations of the solid earth. However, researches on this topic have not gone too far yet.

A more detailed description of the time-variable signals can be found in (Peters, 2007) and (Horwath, 2007). As this thesis deals with mass variations in the ocean, all other signals have to be removed from the integral GRACE signal, which is mainly done in form of models.

2.1.3 Reduced models

The following background models have been reduced during processing of the ITSG-Grace2014 solution.

- IERS 2003 ... Earth rotation
- IERS 2010 ... Earth tide, pole tide and relativistic correction
- EOT11a ... Ocean tide
- Deasi 2003 ... Ocean pole tide
- Bode, Biancle 2003 ... Atmospheric tides (S1,S2)
- AOD1B RL05 ... Atmosphere and Ocean Dealiasing

- JPL DE421 ... Moon, sun and planets ephemerides

In the post-processing, further models have to be removed from the GRACE data depending on the desired signal. Chapter 4 deals with the extraction of the oceanic signal and the necessary models. As only the de-aliasing is of higher relevance when trying to capture the pure oceanic signal out of the gravity field solution, this model will be explained in more detail.

De-aliasing model AOD1B

Because of the characteristics of the GRACE mission a global coverage is first achieved after 30 days, leading to the GRACE monthly solutions. Consequently, signals with periods of less than 30 days are causing disturbing forces which have to be taken into account during the orbit integration as otherwise aliasing effects would occur. Temporal aliasing leads to an appearance of signals with no geophysical background in the time-variable field. To prevent this from happening, a so called de-aliasing model, including high frequency atmospheric and oceanic mass variations, is used during the processing of GRACE gravity field solutions. As mentioned before, the de-aliasing model AOD1B RL05 (*Atmosphere and Ocean De-aliasing Level-1B Release 05*) (Flechtner, 2007) from the GeoForschungsZentrum Potsdam has been used during the processing of the ITSG-Grace2014 solution.

The de-aliasing data is available in spherical harmonics up to degree 100 in an interval of 6 hours. The AOD1B RL05 includes four components *atm*, *ocn*, *glo* and *oba* which describe the gravity change related to a mean field (2000 - 2001). Through this, long-term mass induced trends won´t be taken into account (Gruber and Flechtner, 2007), hence the mass conservation of the AOD1B can be ensured. The *atm* component contains the atmospheric changes in mass, i.e. the atmospheric contribution to the ocean bottom pressure (OBP). *ocn* includes the oceanic contribution to the OBP, *glo* represents the sum of *atm* and *ocn*, that is the global OBP both over land and water. The *oba* component differs from *glo* as all values over land are set to 0. Furthermore not the vertical integrated atmospheric pressure (like for the *atm* component) was taken here, but the atmospheric surface pressure, resulting only in a vanishingly low difference.

Applying the de-aliasing model will remove the atmospheric and the oceanic signal from the gravity field. For investigations of the full ocean signal, the ocean bottom pressure component *oba* has to be added back to the monthly gravity field solutions. To do so, the monthly mean products GAA, GAB, GAC and GAD are available, including the monthly mean values of the *atm*, *ocn*, *glo* and *oba* components. The background model for the AOD1B ocean components is the OMCT (*Ocean Model for Circulation and Tides*), for the calculation of the atmospheric component different atmospheric fields have been considered. Further information on the AOD1B RL05 can be found in the product description document (Flechtner, 2007).

2.2 Post-processing

Working with monthly GRACE solutions, further post-processing steps have to be applied until the solution is ready to use for investigations. This section deals with the steps made in order to gain GRACE data that is ready to work with.

2.2.1 Ocean bottom pressure

In the field of oceanography mass variations in the ocean are basically described using the term of *Ocean Bottom Pressure* (OBP), mainly in combination with the dimension of hPa. OBP defines the pressure of both water and air column along the plumb line acting on one particular point at the ocean´s seafloor. Hence it combines both water masses in the ocean and overlying atmospheric masses. Ocean bottom pressure is determined by

$$p_b(\theta,\lambda,t) = \int_{z=-H_b}^{H_s} g(\theta,\lambda,t)\rho(\theta,\lambda,t)dz + p_s(\theta,\lambda,t) \tag{2.11}$$

$$\approx g_0\rho_0 H_s + g_0 \int_{z=-H_b}^{0} \rho(\theta,\lambda,t)dz + p_s(\theta,\lambda,t).$$

p_s defines the air pressure at sea-level, z is the mean resting sea surface and H_s is the water depth related to z. Assuming the ocean is a thin surface layer, ρ can be set ρ_0 and g can be approximated with g_0, yielding the simplified equation 2.2.1.

To receive ocean bottom pressure anomalies from GRACE spherical harmonics,

$$\Delta OBP(\phi,\lambda) = \frac{ag\rho_E}{3}\sum_{n=0}^{\infty}\sum_{m=0}^{l}\frac{(2n+1)}{1+k_l}P_{nm}(\cos\theta)[\Delta c_{nm}\cos m\lambda + \Delta s_{nm}\sin m\lambda] \tag{2.12}$$

has to be applied (Wahr, 2002). ρ is the mean density of the earth (generally a value of 5517 $\frac{kg}{m^3}$ is assumed), a defines the semi-major earth axis, g the mean gravitational acceleration and k_l is the so-called load Love number that represents the response of the solid earth on surface loads.

2.2.2 Filtering

To detect an interpretable signal in the monthly solutions after subtracting the static field, the use of a filter is necessary as the typical north-south orientated GRACE stripes, induced through the north-south orbiting character, make the detection of a signal impossible. To reduce the errors, different filters can be applied. The most frequently used filter is the isotropic Gaussian filter, but also the so called de-striping filter (Swenson and Wahr, 2006) is already in use regularly.

Gaussian filter

The isotropic Gaussian filter is the most prevalent method used to reduce the systematic errors. The term isotropic refers to the fact that the filter is direction-independent, i.e. it acts the same for all directions. For the filtering in the spectral domain the spherical harmonic coefficients have to be multiplied with the filter coefficients

$$V_F(x) = \frac{GM}{R}\sum_{n=0}^{\infty}\sum_{m=-n}^{n} w_n a_{nm} Y_{nm}(x). \tag{2.13}$$

The filter coefficients are determined in the following way:

$$w_0 = 1 \tag{2.14}$$

$$w_1 = \frac{1 + e^{-2b}}{1 - 2^{-2b}} - \frac{1}{b} \tag{2.15}$$

$$w_n = -\frac{2n - 1}{b} w_{n-1} + w_{n-2} \tag{2.16}$$

with

$$b = \frac{\ln(2)}{1 - \cos(\frac{d}{R})}. \tag{2.17}$$

The crucial factor on the result of the smoothing procedure is the choice of the filter radius d. A filter radius too small will lead to the circumstance that the effect of smoothing is too minor to be able to detect any underlying signal. Applying a Gaussian filter with filter radius too vast will not only diminish the stripes, but also a great part of the actual signal. Depending on the scale of the evaluating signal an appropriate filter radius has to be defined. For global applications and for the evaluation of continental signals a radius of 300 km is mostly sufficient to make a signal visible. The correlation between the applied filter radius and the spherical harmonic coefficients is shown in figure 2.1. Having a look at this figure, it can easily be stated that an increasing filter radius leads to a decrease in the spatial resolution.

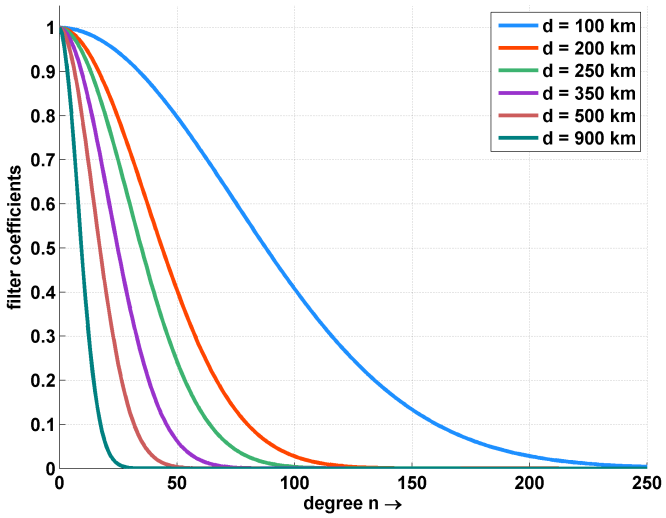

Figure 2.1: Gaussian filter radius

2.2.3 Replacement of GRACE derived coefficients and consideration of GIA

Moreover the degree 1 coefficients (geocenter motion) and the degree 2, order 0 (earth´s flattening) coefficient have to be replaced before working with the GRACE monthly solutions. The degree 1 coefficients are 0 by definition for the GRACE solution, as GRACE is measuring in the CM (center of mass) frame. When comparing the GRACE data with models, such as the ESA ESM, the geocenter motion has to be taken into account by replacing these coefficients (Swenson et al., 2008). The C20 GRACE coefficient is basically

replaced by a C20 coefficient determined by SLR (*Satellite Laser Ranging*), as this one is less noisy. Also the GIA effect must be considered when working with GRACE data sets. More on the topic of replacing these coefficients and the consideration of the GIA effect can be found in chapter 4.

2.3 Analysis

For the analysis of satellite gravity data a great selection of appropriate tools is available. This section only lists and describes those that have been worked with during this thesis.

2.3.1 RMS

One of the most useful tools in determining variations in the time-variable gravity field is the RMS (*Root Mean Square*) which is defined through

$$rms = \sqrt{\frac{1}{N}\sum_{i=1}^{N}(f(t_i) - \overline{f})^2}. \tag{2.18}$$

$f(t_i)$ is a functional of the gravity field, in our special case OBP, given over a distinct time span, $\overline{f}$ represents the mean value of this time series and N is the total number of values. Applying equation 2.18 on a gridded data set, the mean value of the squared deviations at each grid point is computed. This yields a map of RMS values showing irregularities in the time-variable gravity field.

2.3.2 EOF

The EOF (*Empirical Orthogonal Function*) analysis is frequently used in spatial analysis of GRACE data to detect significant spatial patterns. Based on orthogonal functions that can be determined through the given data, a decomposition of the signal takes place to identify patterns of temporal variations. The concept of the EOF analysis is the so called singular value decomposition. For the decomposition all the data that shall be taken into account in the EOF analysis has to be assembled in one matrix. This matrix has to be arranged so that the rows represent the temporal development and the columns the different grid points. In other words, a column of this matrix contains all available grid points at one distinct instant of time and a row shows the temporal progress of one particular grid point. A more detailed explanation and the formulas used in EOF analysis can be found in (Hannachi, 2004). The result of the singular value decomposition is a matrix, whichs columns include the various EOF modes. These modes show the different existing spatial patterns with a certain percentage of the total variance of the signal, called the explained variance, with λ being the eigenvalues

$$k = \frac{\lambda_k}{\sum_{i=1}^{n}\lambda_i} \cdot 100. \tag{2.19}$$

The first mode represents the strongest pattern and is therefore having the highest explained variance. Beside the spatial patterns also temporal patterns are produced during the EOF analysis, called the principal components PC. The principle components are

uncorrelated and are showing the amplitude of the EOF patterns as a function of time. Beside the detection of spatial patterns the EOF analysis is sometimes also done in the sense of data reduction or filtering. The filtering is done by reconstructing the signal only by the first modes with the highest explained variance, as the noisy part of the signal usually has a low explained variance.

As the EOFs provide a purely statistical compression of the data field, the physical interpretation of the patterns has to be done with caution. Basically only the first mode (or the first few modes, according to the corresponding explained variance) shall be physically interpreted, preferably in combination with the attendant principal components. The difficulty in interpreting the EOFs in terms of physical processes is because of the EOFs property of being orthogonal and uncorrelated. In reality, physical processes are neither compulsory orthogonal (Simmons et al., 1983) nor uncorrelated (von Storch and Zwiers, 1999), hence it complicates their interpretability.

2.3.3 Degree variances

Degree variances are representing the signal content per degree or in other words, they define the spectral power density of the function over the surface of a sphere. According to the Kaula rule of thumb, the signal content is decreasing with increasing degree. The often used term of *degree amplitude* refers to the square root of the degree variances. The computation of degree variances is done as follows

$$c_n^2 = \sum_{m=0}^{n} (c_{nm}^2 + s_{nm}^2). \tag{2.20}$$

Here the so-called *Signal-RMS* respectively the average degree amplitude is basically used, which defines the average signal content per degree

$$c_n = \sqrt{\frac{1}{2l+1} \sum_{m=0}^{n} (c_{nm}^2 + s_{nm}^2)}. \tag{2.21}$$

Error degree variances provide information on the accuracy of the spherical harmonic degrees:

$$\sigma_n^2 = \sum_{m=0}^{n} (\sigma c_{nm}^2 + \sigma s_{nm}^2). \tag{2.22}$$

Degree and error degree variances are primarily used to evaluate gravity field solutions regarding their achievable accuracy. The intersection of the degree variance curve and the error degree variance curve marks the point where the noise is exceeding the signal content. From the use of degree and error degree variances one can imply the scale of detectable signals in the corresponding gravity field solution.

3 The updated ESA ESM

The modeling of our system earth is an important part in the field of climate research as it helps us to understand the system as a whole as well as the interaction between its various subsystems. The melting of continental ice masses (cryosphere) leads to a rise of the sea-level (hydrosphere), variations in the atmosphere result in variations in the ocean, just to name a few of these interactions between the spheres. But also the processes within one sphere are of great interest, e.g. ocean currents, change in glaciers, deformations in the earth´s crust and more. Earth System Models are therefore used in the progress of setting up new satellite missions that aim to measure mass transports on and beneath the earth´s surface. These models simulate known mass transport processes that might be measured by the satellite gravity mission and can thus be employed to investigate the concept of future satellite gravity missions. One such model is the so called *updated ESA Earth System Model* (ESA ESM) which was set up by the *GeoForschungsZentrum Potsdam* (GFZ) in August 2014 (Dobslaw et al., 2014). The following sections deal with the concept of the model as well as its components.

3.1 The model

Since August 2014 the updated ESA ESM, a revised version of the original ESA ESM (Gruber et al., 2011) has been available. As the original ESA ESM, which has been in use since 2011, showed some shortcomings, an update of the model has been induced. Several smaller changes have been adapted (Dobslaw et al., 2014). The most striking modification however is the usage of the so called inverse barometer correction (*IB correction*) which induces a relief in the interpretability of the ocean component.

The model is provided by the GFZ and describes the time-variable part of the earth´s gravity field. Referring to the various subsystems of the earth, the model is composed of five representative components (A, O, H, I and S) which are given in the form of spherical harmonics until degree 180. All components are given in the CF (*center of figure*) frame and are represented in form of surface density variations.

In total a time span of 12 years (1995 to 2006) is covered with a temporal resolution of 6 hours whereby the coefficients are given at the exact instant of time 00:00, 06:00, 12:00 and 18:00 UTC. In addition to this model also a de-aliasing model (Dobslaw et al., 2015) will be provided in order to remove high-frequency non tidal induced mass movements during the processing of satellite gravity data.

3.2 The components

The updated ESA ESM is, like the original ESA ESM, given in form of five distinct components, denoted as A-, O-, H-, I- and S-Component. Each component comprises the

mass variations of a solitary subsystem of the earth. The following listing shall give an overview of the comprised mass variations.

- A ... inverse barometrically corrected atmospheric variability
- O ... inverse barometrically corrected ocean bottom pressure variability
- H ... variability in the terrestrial water storage
- I ... variations in continental ice shields and glaciers
- S ... variations in the solid earth resp. post glacial rebound and co- and post seismic deformations

The components are provided individually as well as in combination (AOHIS) and can be downloaded from FTP-Server of the GFZ Potsdam[1]. In the directory *mtmshc* the individual components, as well as the combination AOHIS can be found at a temporal resolution of 6 h. Furthermore also even higher-resolutional data for the year 2006 is available (*mtm3h*) and an additional atmospheric component, the AnoIB component (*mtmnIB*). AnoIB contains the not inverse barometrically corrected atmospheric variability with the same spatial and temporal resolution as the data in *mtmshc* The difference between the A and the AnoIB component will be demonstrated later. Beside the model components the de-aliasing model and the corresponding error are available in the (*mtmdeal*) directory.

Each of the given components has a different underlying model. A rough overview of those background models is given in 3.1.

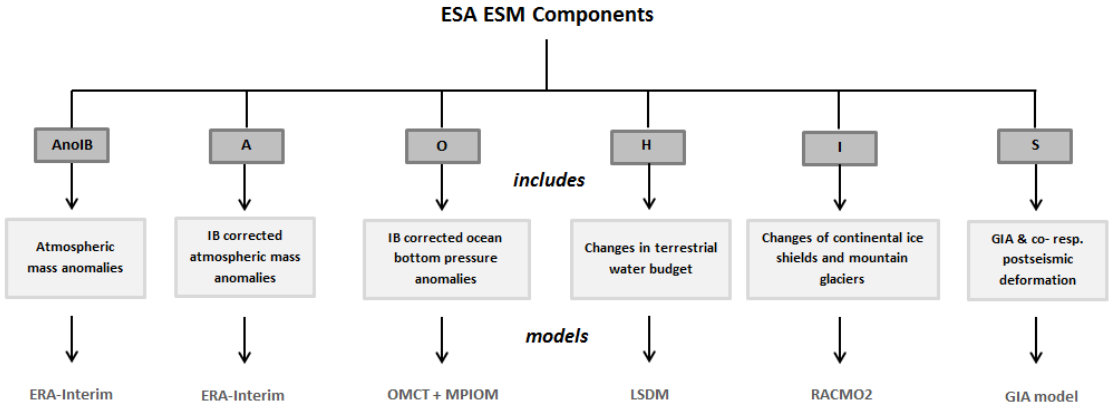

Figure 3.1: Contents and background models of updated ESA ESM components

As the focus of this thesis lies on the mass variations in the ocean, only the ocean component (O) will be described and discussed in more detail. More information on the other components can be found in the definition document of the updated ESA ESM (Dobslaw et al., 2014).

[1] `ftp://ig1-dmz.gfz-potsdam.de/`

3.3 The ocean component

Starting with numerical simulations the total ocean bottom pressure, composed of oceanic and atmospheric contribution, is estimated. According to the IB correction the atmospheric surface pressure mean field, averaged over all oceanic areas, has to be removed from the estimated data. Additionally, further steps have to be made in order to arrive at OBP anomalies. Figure 3.2 demonstrates those steps.

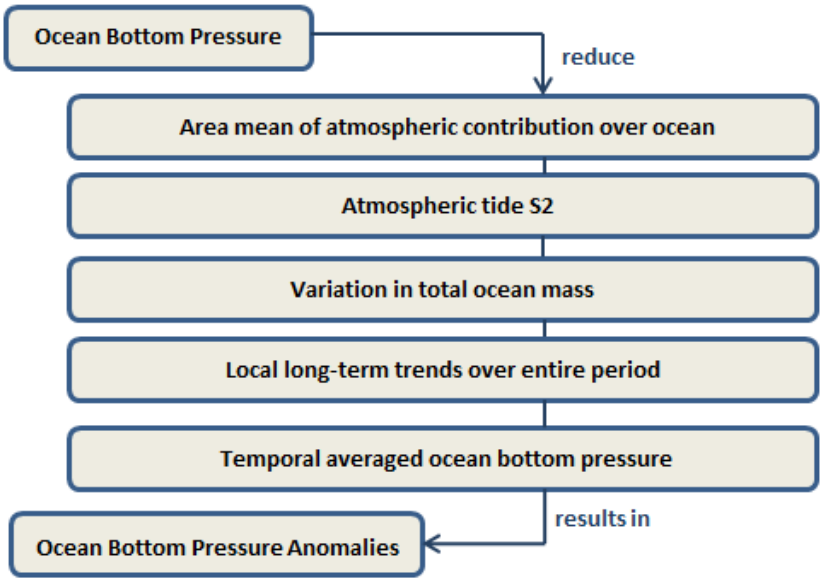

Figure 3.2: Detailed composition of the oceanic component

3.3.1 Background models

Simulating ocean mass transports, the O component can be used for geophysical interpretations of ocean processes. Depending on the spatial and temporal resolution of the background models, the visibility of distinct scaled processes varies. For the oceanic component of the updated ESA ESM two different background models were used. On the one side there is the baroclinic OMCT (*Ocean Model for Circulation and Tides*), and on the other side the ocean component MPIOM (*Max-Planck-Institute for Meteorology Ocean Model*) of the climate model STORM (*German consortium for the development of a very high resolution climate model*). Ocean models are often classified according to whether they ignore (barotropic model) or include (baroclinic model) density variations in the ocean. The terms *baroclinic* and *barotropic* are further described in section 5.1.3. As baroclinic models are barely calculating thermohaline and wind driven signals (Thomas and Dobslaw, 2004), barotropic processes might not be entirely resolved (Hughes et al., 2007).

The OMCT (Thomas, 2002) is progressed out of the HOPE (*Hamburg Ocean Primitive Equation*) (Drijfhout et al., 1996; Wolff et al., 1997) model and is based on the non linear impulse equation as well as the preservation of salt, heat and mass under the usage of the hydro static and the Boussinesq-approximation (simplified consideration of horizontal

mass transports). The temporal resolution of the model is 30 minutes, reduced to six hour time steps for the ESA ESM O. The spatial resolution of the model is limited to 1.0°, thus only large-scale ocean variability can be resolved. As the spatial resolution of the OMCT is not sufficient to resolve ocean processes at smaller scales, an additional ocean model is used within the updated ESA ESM. The MPIOM (Jungclaus et al., 2013) is the ocean-sea ice model developed at the Max-Planck-Institute of Meteorology that is used as ocean component in the climate model STORM. Admittedly the model is only given at a lower temporal resolution of one day, however it has a much higher spatial resolution of 0.1° and is therefore even eddy resolving.

Composition

Regarding the characteristics of the currently described ocean models the data sets are combined in the spectral domain, where the lower spherical harmonics are taken from the OMCT ($\leq$ d/o 60) and the spherical harmonics of degree 61 - 180 are contributed by the MPIOM. As mentioned before, the updated ESA ESM aims to preserve the total mass of the earth. Mass flows between the subsystems have nevertheless been taken into account as the melting of continental ice masses in Greenland (I component) results in changes in the total ice mass as well as the ocean mass (O component). Because of such inflows of external water masses, the ocean reacts with a global change in the ocean bottom pressure field, the total ocean mass changes and therefore the sea-level rises. This variation is called eustatic sea-level anomaly and its consideration is essential as it plays an important role in the contribution to global sea-level rise. To account for the eustatic variability in the ocean and simultaneously keeping the total mass of the earth constant, the negative anomalies in total mass of the A, I and H component is accumulated at each time step and added to the total ocean mass. An overview on the composition of the oceanic component is given in figure 3.3.

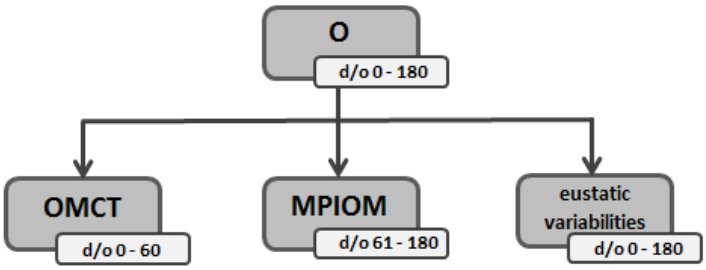

Figure 3.3: Constitution of O component

3.3.2 Inverse barometer effect

The greatest difference between the original and the updated ESA ESM is the use of an IB correction. As this mainly affects the ocean component of the model, this section shall explain the phenomena of the inverse barometer effect.

Although both subsystems ocean and atmosphere could be considered as delimited and independent systems, they are typically denoted as a dynamical coupled system as they

affect each other quite strongly. On the one hand side the atmosphere affects the ocean in terms of solar radiation that influences the ocean circulation. The ocean in turn operates as a heat accumulator that urges the atmospheric circulation. Briefly speaking, the atmosphere drives the ocean, the ocean the atmosphere.

Also the existence of high and low pressure fields in the atmosphere influences the underlying ocean. The sea surface is (almost) directly reacting on anomalies in the atmospheric pressure field. An increase in the atmospheric pressure leads to a reduction in the sea-level, in case of mitigation of atmospheric pressure the ocean´s surface height will increase. This particular behavior of the ocean, reacting on changes in the atmospheric pressure field, is called the *inverse barometer effect*. This results in a coupled system, whichs separation is nevertheless essential for simulating purposes to observe mass anomalies in the ocean not induced by the atmosphere. The change of the sea-level due to the inverse barometer effect can be expressed by the following equation:

$$\zeta^{IB} = -\frac{\delta p_a}{p_0 g} \tag{3.1}$$

with δp_a being the change in pressure, p_0 the density of water and g the gravity acceleration. A more detailed description of the inverse barometer effect can be found in (Wunsch and Stammer, 1997).

Oceanic mass variations are typically expressed in ocean bottom pressure which per definition is the accumulated effect of the hydro static pressure of atmospheric and oceanic masses along the plumb line over one particular point on the ocean floor. For the global representation of ocean bottom pressure the oceanic and the atmospheric contribution to the ocean bottom pressure is usually split up. If the inverse barometer effect is not considered here, then the oceanic part only reflects the slightly delayed response of the ocean to atmospheric pressure changes. Figure 3.4, which depicts the oceanic and the atmospheric component of the de-aliasing model AOD1B, outlines this effect very well.

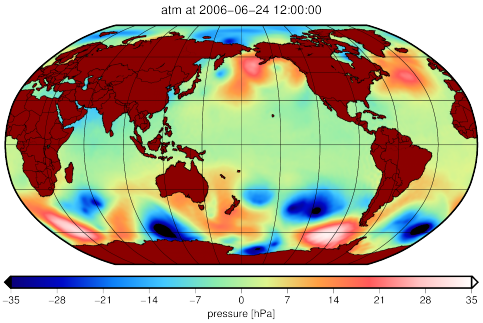

(a) Non IB-corrected atm component of AOD1B at 2006-06-24 12:00:00

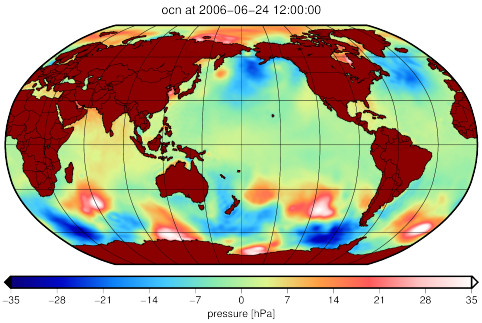

(b) Non IB-corrected ocn component of AOD1B at 2006-06-24 12:00:00

Figure 3.4: Inverse barometer effect in AOD1B components

If no IB correction is applied to the single components, no distinct statement can be given on eventual mass variations in the ocean as barely the impact of the atmosphere is mirrored. To avoid this, an IB correction is applied in the updated ESA ESM. It has to be stressed, that this correction does not influence the ocean bottom pressure as a whole, it only eliminates the correlation between ocean and atmosphere. To conduct this

correction the time-variable part of the atmospheric contribution to ocean bottom pressure e.g. the difference between the mean surface pressure field (averaged over the ocean) and the actual atmospheric surface pressure has to be added to the oceanic component. In return, the same sum has to be removed from the A component, leading to a replacement by the mean atmospheric surface pressure field. This implementation brings about the fact that the sum of A- and O- component of the IB corrected updated ESA ESM is equal to those components of the original ESA ESM, as the original ESA ESM does not apply this correction. The IB correction only matters for the separation of oceanic and atmospheric contribution to ocean bottom pressure. For oceanographic applications it simplifies the interpretation of mass movements in the ocean as the correlation of ocean and atmosphere has been removed. The effect of the IB correction of the components can be seen in 3.5.

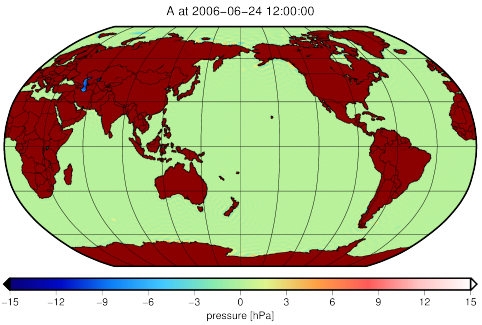

(a) IB-corrected atmospheric component from updated ESA ESM at 2006-06-24 12:00:00

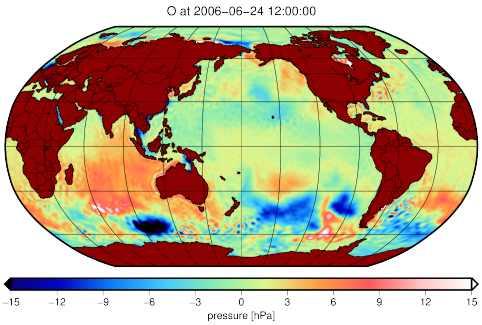

(b) IB-corrected oceanic component from updated ESA ESM at 2006-06-24 12:00:00

Figure 3.5: Effect of IB correction

The A component solely contains the rather small static part of the atmospheric contribution to the ocean bottom pressure. The O component consists of the oceanic contribution as well as the variable part of the atmospheric contribution to the OBP.

4 Global sea-level change

The first emphasis of this thesis lies on the evaluation of eustatic sea-level variations from satellite gravity data (GRACE) as well as from model data (ESA ESM) and their comparison. The calculation of eustatic sea-level changes from satellite gravity data requires far more effort than the computation from model data and will be discussed in detail. The following sections will first give a short introduction to the topic of global sea-level change and will then point out the differences and steps in determining the eustatic sea-level variations that have to be executed in order to guarantee the comparability of the results from both data sets.

4.1 Sea-level rise

One of the most discussed subjects concerning climate change is the rise of the sea-level, as it will influence the majority of the earth´s population. The total sea-level rise lies around 3 mm per year, permanently increasing during the last years (Church et al., 2013). Using the term *sea-level rise*, it basically has to be differentiated between the two different contributing effects, the eustatic and the steric one. The eustatic sea-level rise describes the global homogeneous rise of the sea surface due to changes in the oceanic mass e.g. through the melting of glaciers and continental ice sheets. Those processes are typically on short time scales and can proceed comparatively quickly. Beside this, also the impact of ocean seafloor spreading that brings along a change in the oceans volume belongs to the eustatic effect. The more long-range consequence of climate change is the steric sea-level rise, whose main reason is global warming. Already available water in the ocean expands in consequence of warming, resulting in an increase of the sea-level. This effect is also called thermosteric effect, as it only depends on changes in the oceans temperature.

The eustatic sea-level rise can be determined by satellite gravity missions such as GRACE, as it concerns mass changes whereas the steric effect won´t be seen in satellite gravity data as no modifications in the ocean mass will take place. With the use of altimeter satellites the total sea-level rise can be determined and through a reduction of the eustatic contribution the steric effect can be calculated. More detailed information on the topic of global sea-level rise can be found in (Church et al., 2013).

4.2 Data sets

The two different data sets used within this investigation are the gravity field solution ITSG-Grace2014 from the Institute of Geodesy in Graz and the oceanic component (*O component*) from the updated ESA ESM. Table 4.1 lists the most important properties and differences of the given data sets.

Table 4.1: Characteristics of input data

	ESA ESM O component	**ITSG-Grace2014**
time interval	6 h	monthly mean
d/o	0 - 180	0 - 120
period	1995 - 2006	2003 - 2014
reference epoche	mean field from 1995-2006	2008-01-01
reference frame	CF	CM

As the ITSG-Grace2014 gravity field solutions are only available at monthly means, the ESA ESM data, which is obtainable in 6 hour time steps, has to be averaged to monthly means as well for the computations. The results for both data sets are uniformly given in equivalent water height (EWH) per mm.

4.3 Eustatic sea-level change from GRACE

As the eustatic sea-level change is equivalent to the total change in ocean mass, GRACE is able to observe this phenomenon. The main difficulty in using GRACE data for the analysis of one particular process on earth, is the superposition of all present mass induced signals. Hence a separation of those signals has to take place prior to the detection of the eustatic sea-level change. Beside this, some GRACE sourced peculiarities have to be taken into account as well. All in all, the following steps have to be regarded in order to gain a satisfying result of the eustatic sea-level variation:

- remove the glacial isostatic adjustment (GIA) by the use of a model
- add the de-aliasing model removed during processing of GRACE data
- apply an appropriate filter and
- a land-ocean-mask
- replace the C20 coefficient
- as well as the degree 1 coefficients and
- consider the loading

4.3.1 Glacial Isostatic Adjustment

The *post glacial rebound* (PGR) or *glacial isostatic adjustment* (GIA) names the effect that occurs due to the loading of ice masses on the earth´s crust during the ice ages. Over centuries kilometer thick ice layers have been positioned on the land masses, especially in northern Europe (Fennoscandia), Siberia and North America, resulting in a dent of the underlying crust. Mantle material has therefore been urged outwards, where the crust consequently bulged. With the melting of the ices masses the converse scenario took place, mantel material flowed back and is causing the crust to lift back to its original state. This still ongoing process is called the glacial isostatic adjustment.

As the GIA is a long-term mass induced signal, GRACE does measure this signal. Consequently this signal has to be removed from the gravity data set in order to gain the pure ocean mass signal. Several models have been developed in order to reduce this event from satellite gravity data, their statements on the annual trend though vary between 1 mm per year (Paulson and Wahr, 2007) and 2 mm (Peltier, 2009) with a model uncertainty of 20 %[1]. Here the *GIA_Klemann2008* model with an annual trend of 1 mm per year (Klemann et al., 2008) has been used. According to the yet quite large differences between the GIA models the use of a particular model strongly influences the evaluation of the eustatic sea-level variations. Not accounting for the GIA at all during the calculations leads to a grave false result like visible in figure 4.1, as no trend in the total global ocean mass is apparent.

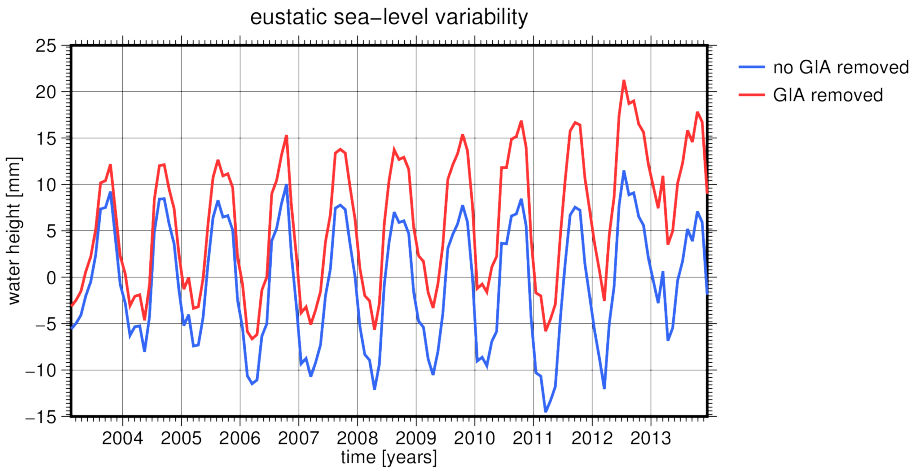

Figure 4.1: Impact of GIA on evaluation of eustatic sea-level variability

Thus the GIA has the largest effect on the result of eustatic sea-level estimation when this signal is not correctly removed from the GRACE data.

4.3.2 De-aliasing model

During the processing of the satellite gravity data from GRACE, a de-aliasing model has been removed in order to reduce aliasing effects from high frequency ocean and atmosphere signals. To restore the entire ocean signal, the oceanic part of the de-aliasing model has

[1] http://grace.jpl.nasa.gov/data/get-data/gia-trends/, accessed 2015/05

to be added back to the GRACE monthly solutions. With this step also the separation of the atmospheric signal, which as well overlies the oceanic signal, is accomplished. The de-aliasing model used during the processing of the ITSG-Grace2014 solution is the previously described AOD1B RL05. For the comparability with the IB corrected oceanic component of the ESA ESM, the *oba* component of the AOD1B, including the ocean bottom pressure over the ocean, has to be added back to the GRACE data. During this step one has to pay attention to the circumstance that both the degree 0 and degree 1 components have not been reduced from the GRACE data while the processing step. Therefore these coefficients should generally not be added back to the monthly solutions (Gruber and Flechtner, 2007). However, because the geocenter motion has to be considered here as well, the degree 1 coefficients of the *oba* de-aliasing component should after all be added to the monthly solutions. More on the subject of geocenter motion and the importance of its consideration will be discussed in the subsequent section 4.3.3.

The necessity of not including the degree 0 coefficients from the AOD1B RL05 de-aliasing model is depicted in figure 4.2. As the C00 coefficient is basically referring to the total mass, a change in total mass is observable through this coefficient. With GRACE the temporal displacement of masses can be measured, nevertheless the total global mass won´t change at any time step as no mass is leaving the earth. Observing only one single subsystem of the earth, e.g. the ocean, the total mass of this subsystem must not stay constant due to interaction with other subsystems. This case applies for the de-aliasing model resp. its ocean bottom pressure component. The figure shows the difference between the C00 coefficient of the ITSG-Grace2014 gravity field solution and the C00 coefficient of the *oba* de-aliasing component. The temporal variation of the C00 coefficient of the ITSG-Grace2014 solution is constantly 0, as expected. For the *oba* component however, the C00 is varying with time, as it only represents the ocean mass, which does not mandatorily have be constant.

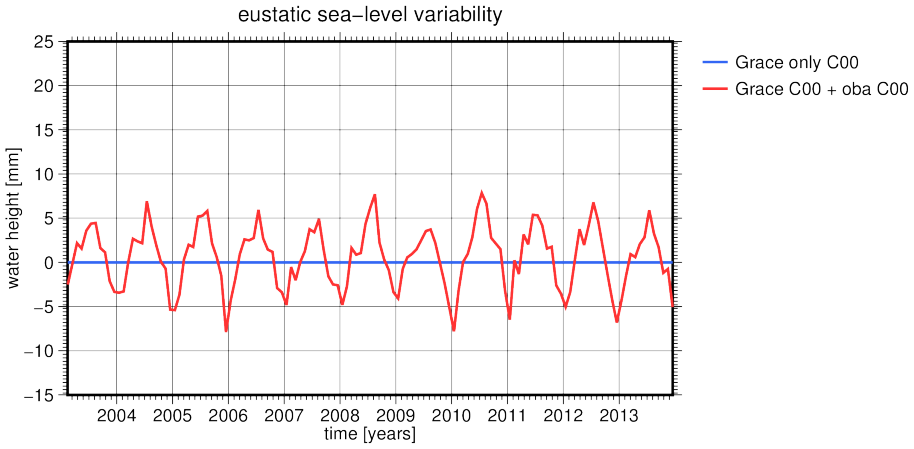

Figure 4.2: Impact of de-aliasing C00 coefficient on eustatic sea-level variability

Figure 4.2 shows, that the coefficient is changing between +5 mm and -5 mm in amplitude and clarifies the necessity of neglecting the coefficient C00 in the back addition of the de-aliasing model.

4.3.3 Replacement of GRACE coefficients

The replacement of GRACE coefficients affects the C20 coefficient, characterizing the earth´s flattening, and the degree 1 coefficients which per definition describe the geocenter motion. Because of errors in the models of diurnal and semi diurnal ocean and solid earth tides, aliasing effects appear in the lower spherical harmonics and especially the zonal C20 coefficient[<2>]. This is why the C20 coefficient is usually replaced by a SLR determined C20 coefficient that is less noisy than the GRACE derived one. The SLR C20 time series for the replacement is obtained from the *Physical Oceanography Distributed Active Archive Center* (PODAAC) via `ftp://podaac.jpl.nasa.gov/allData/grace/docs/TN-07_C20_SLR.txt`. This file includes the mean C20 coefficient for each month in the time period from 2001 until 2014. After replacing the coefficients in the GRACE monthly solutions, monthly means have been computed (missing GRACE months have been interpolated) for further investigations. The effect of the replacement on the eustatic sea-level change can be seen in figure 4.3.

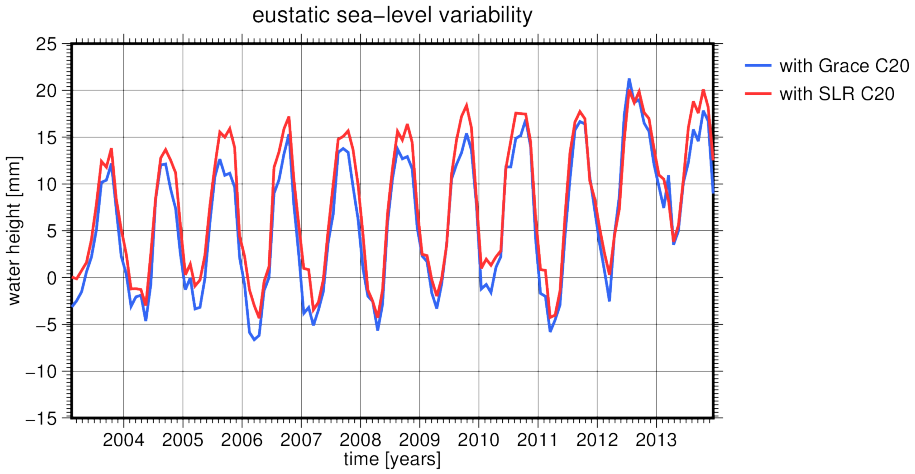

Figure 4.3: Impact of replaced GRACE C20 coefficient on eustatic sea-level variability

As the GRACE mission is referred to the CM (*Center of Mass*) frame, the spherical harmonics coefficients of degree 1 are 0. The model data of ESA ESM are though present in the CF (*Center of Figure*) frame, hence the geocenter motion has to be taken into account in order to compare the results of both data sets. Consequently, the GRACE degree 1 coefficients have to be replaced. This has been done using the coefficients from `ftp://podaac.jpl.nasa.gov/allData/tellus/L2/degree_1/deg1_coef.txt`, which have been computed by the method of (Swenson et al., 2008). Those coefficients however merely represent the land component of the degree 1 gravity field coefficients. To acquire the global degree 1 coefficient, the oceanic degree 1 coefficients have to be added as well, which is done by adding the degree 1 coefficients of the AOD1B RL05 (like mentioned in the previous section).

Comparing the figures 4.3 and 4.4, the effect on the estimation of eustatic sea-level variations is bigger for the replacement of the C20 coefficient. Accounting for the geocenter motion has only a small effect on global scale. For regional applications however it is of

[2] http://adsabs.harvard.edu/abs/2008AGUFM.G13A0632R, accessed 2015/03

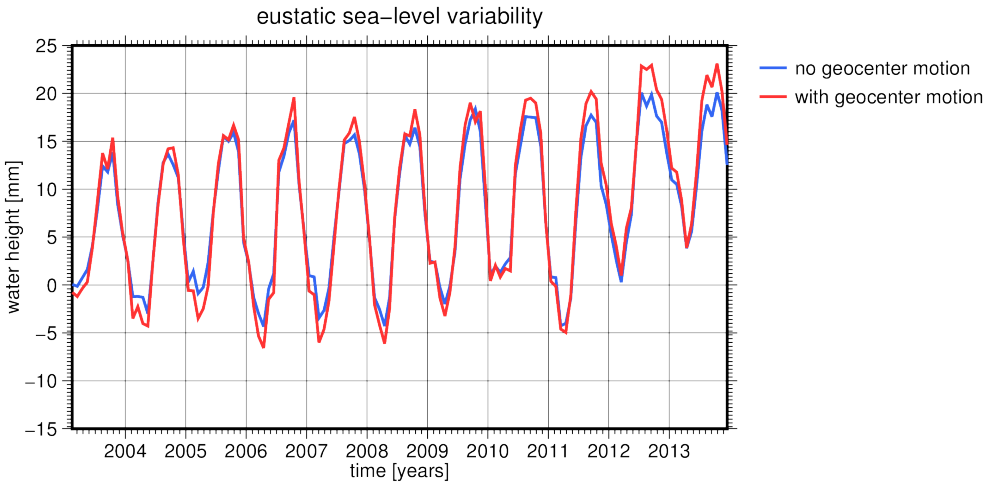

Figure 4.4: Impact of replaced GRACE degree 1 coefficients on eustatic sea-level variability

greater importance to consider geocenter motion.

4.3.4 Filtering and land leakage

To gain an interpretable time-variable gravity field from GRACE, the monthly solutions have to be filtered in order to remove systematic errors visible in form of the typical GRACE north-south stripes. These systematic errors can be diminished through the use of an appropriate filter. The usually applied isotropic Gaussian filter is one possibility, another commonly used approach is the so called destriping filter (Swenson and Wahr, 2006), which nevertheless has to be used in combination with a Gaussian filter. The choice of a suitable Gaussian filter radius is a sensitive issue, as on the one hand it should not be too small so that possible signals won´t stay hidden beneath the stripes, and on the other hand a filter with a Gaussian filter radius being too vast will increase the possibility of land leakage and therefore the distortion of the total ocean mass. Figure 4.5 illustrates the effect of different Gaussian filter radii applied to the ITSG-Grace2014 monthly solutions.

The term land leakage describes the effect of blurring land signal into the ocean signal in the immediate vicinity of coastal areas. In regions with utterly distinct mass trends on land and in the ocean (e.g. Greenland and surrounding area) parts of the land signal can be transferred into the ocean signal leading to a blurring of the true oceanic mass trend. Therefore a proper land-ocean mask has to be used to eliminate data from coastal areas and diminish the effect of land leakage. As a Gaussian radius of 300 km is appropriate to be used for the evaluation of the eustatic sea-level rise a land mask is used, leaving coastal ocean areas within a distance of 3° unconsidered. The omitting of coastal areas using an appropriate land mask has obvious consequences on the global ocean mass as figure 4.6 reveals. Applying no buffer zone, an error of sometimes up to 5 mm in amplitude would occur.

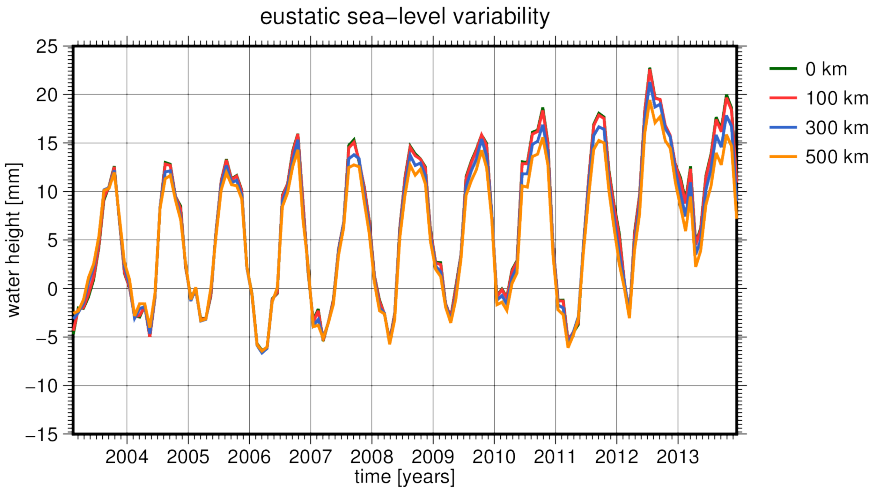

Figure 4.5: Impact of choice of Gaussian filter radius on eustatic sea-level variability

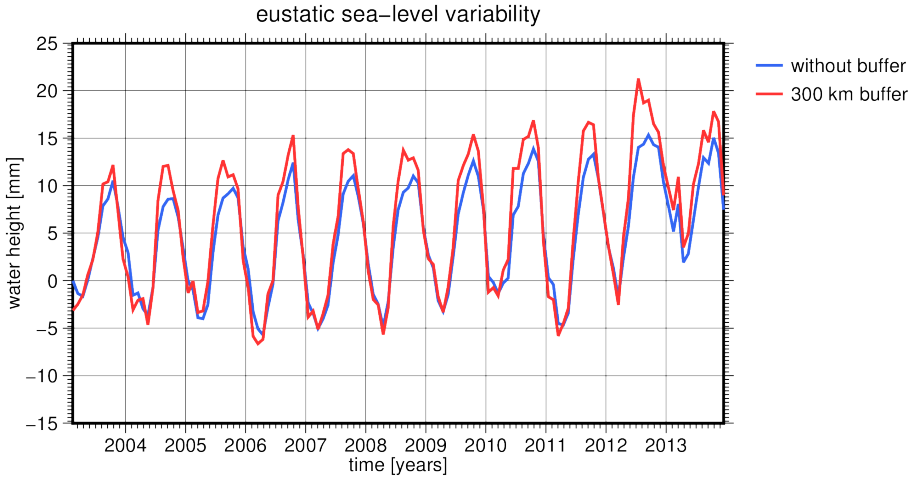

Figure 4.6: Impact of choice of land-ocean mask on eustatic sea-level variability

4.3.5 Loading

Because of the different reference frames (CF in case of the model data and CM in case of the satellite gravity data), also the changes in the degree 1 Load Love Number have to be considered for the computation of the eustatic sea-level rise, as otherwise the deformation of the solid earth would not be taken into account. That is why $k_{1'} = 2.6014 \cdot 10^{-2}$ will be used in the following, although the effect on the total ocean mass is vanishingly small as shown in figure 4.7.

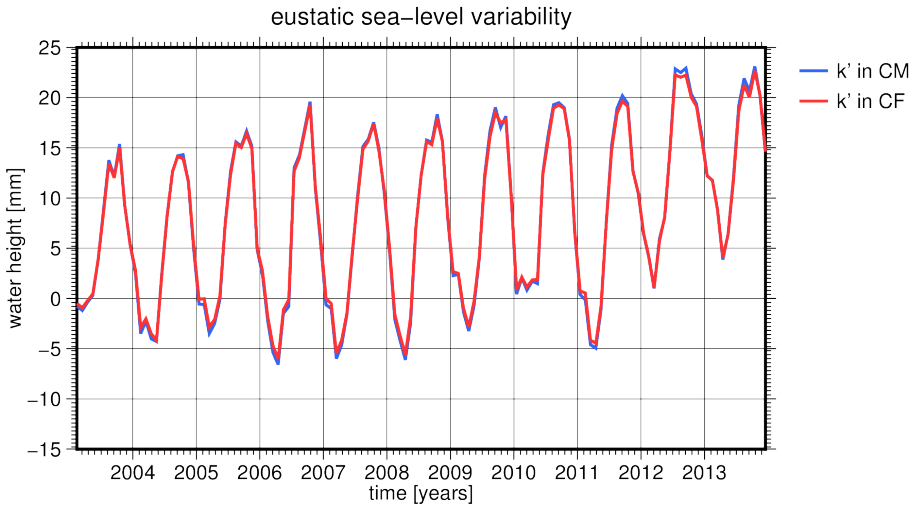

Figure 4.7: Impact of $k_{1'}$ coefficient on eustatic sea-level variability

4.4 Eustatic sea-level change from ESA ESM

For the evaluation of the eustatic sea-level changes from the ESA ESM basically no additional steps have to be applied. However, to account for comparability with the results from the ITSG-Grace2014 data, the same filtering method as well as the same land-ocean mask has to be applied to the model data. Furthermore the spherical harmonics up to degree 60 have been taken into account as well. The result of the ESA ESM derived eustatic sea-level rise is not depicted separately but can be found in the figures when comparing both data sets in the subsequent section.

4.5 Comparison of eustatic sea-level variations

Taking the exact same preconditions for both data sets, the results for the evaluated sea-level rise match almost perfectly like depicted in figure 4.8. Generally the figure reveals that the eustatic sea-level rise started in the year 1998. Before, in the time between 1995 and 1998 it seems like a slight negative trend occurred. In the overlapping period of 2003 - 2006 a good accordance between both data sets is visible, only the range of the amplitude varies a bit in 2003, probably resulting from the comparatively low accuracy of GRACE in this year.

Figure 4.9 reveals the eustatic sea-level rise with the seasonality removed, the obvious increase of the eustatic sea-level is around 1.4 mm/year for the period of 1995 - 2006 (ESA ESM) and 1.0 mm/year in the period from 2003 - 2013 (ITSG-Grace2014). Comparing those results with former research results, it can be seen that the estimates for the eustatic sea-level rise is varying between 1 mm per year to 2 mm per year. Reasons for these discrepancies are multiplex, the usage of various GRACE solutions as well as the use of diverse GIA models and the different evaluation steps play a significant role (Quinn and Ponte, 2010).

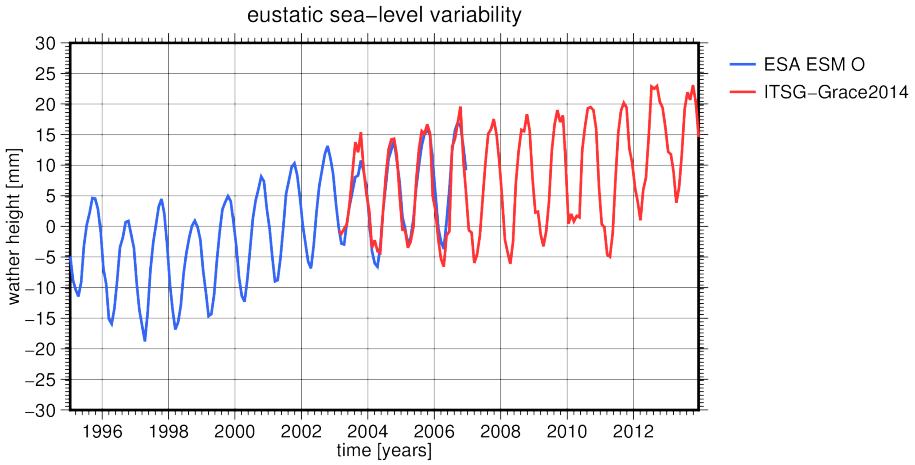

Figure 4.8: Eustatic sea-level variation in the period of 1995 - 2014 from the oceanic component of the updated ESA ESM (d/o 60) and ITSG-Grace2014 monthly solutions (d/o 60) with all former mentioned processing steps applied

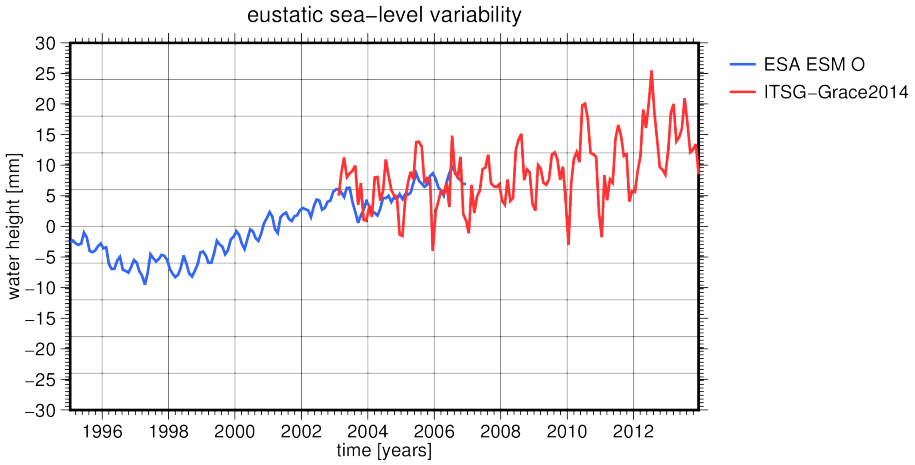

Figure 4.9: Eustatic sea-level variation in the period of 1995 - 2014 from the oceanic component of the updated ESA ESM (d/o 60) and ITSG-Grace2014 monthly solutions (d/o 60) with seasonality removed

5 Meso-scale ocean processes

A great variety of processes exist in our oceans, on different spatial as well as temporal scales. Starting from the ocean tides, representing the strongest ocean signal with a spatial extent over thousands of kilometers, to meso-scale processes, being considerably smaller reaching a spatial scale of only a very few hundreds of kilometers to submeso-scale activities, having diameters less than 10 kilometers. The periods of the various processes cover the whole spectrum, from decadal to diurnal to semi- and even sub diurnal. Using satellite gravity missions such as GRACE, some of these processes can already be observed, helping us to gain a better knowledge on the complex system ocean. However, GRACE has both a limited spatial and temporal resolution, consequently the so called meso-scale processes have remained largely undetected by now. This chapter shall give a short theoretical insight on the topic of meso-scale eddies and the observation regions examined during this thesis.

5.1 Meso-scale processes

To investigate to what extent meso-scale processes can already be observed by GRACE, one has to know what is meant with the definition of meso-scale. Furthermore a theoretical knowledge of the emergence process of eddies and their properties is of advantage.

5.1.1 Definition meso-scale

Unfortunately, the term meso-scale is not definite since several different definitions on this term currently exist. Usually a meso-scale process is defined as a process having a spatial extent of around 10 to 100 km[1]. However, sometimes also the Agulhas rings with diameter of up to 300 km and even processes up to 500 km[2] are sometimes classified as meso-scale. The temporal resolution also varies strongly, lying between some weeks to even half a year. Meso-scale processes occur not only in the ocean, but also in the atmosphere, where they play a great role in the formation of our weather. This is why ocean eddies are sometimes referred as the ocean´s weather. Beside the term meso-scale, also the term submeso-scale appears from time to time, defining processes with a spatial extent between 1 and 10 km. Those activities are hardly understood by now, as their spatial scale is way too small to be observed by satellite missions.

5.1.2 Ocean eddies

Typical meso-scale processes in the ocean are the so called eddies, small circulating currents. Turbulent ocean eddies mainly occur at the edge of vast currents, such as the

[1] http://www.gfdl.noaa.gov/ocean-mesoscale-eddies, accessed 2015/04
[2] http://ctoh.legos.obs-mip.fr/applications/mesoscale/what-are-mesoscale-processes, accessed 2015/04

Agulhas current or the Gulf current due to dynamical instabilities. Structures like meanders start to emerge because of the instability and split off the main current, executing independent circulations. Those separated eddies differ strongly from their surrounding in their properties, as they are characterized by strong temperature-, salinity- and SSH (sea surface height)- anomalies and are basically richer in energy than the current they arose from. In general, even more than half of the ocean´s kinetic energy is said to be saved in ocean eddies[3].

Beside the formation due to dynamical instabilities, eddies can also be formed owing to ocean seafloor obstacles such as underwater mountains. Referred to their formation process, eddies can be classified into transient (formation due to instabilities) and stationary (formation due to obstacles) eddies. Ocean eddies can furthermore also be distinguished according to the direction of their rotation. Cyclonic eddies rotate anti-clockwise on the Northern hemisphere, on the Southern hemisphere the clockwise rotating eddies are described as cyclonic ones. Anticyclonic eddies behave the exact other way round. Depending on a cyclonic or anticyclonic rotation, eddies are cold core rings or warm core rings, conducting vertical water mass transports. According to this, either cold water flows from deep layers to the surface or warm water is transported from the sea surface to the deep ocean as it is depicted in figure 5.1.

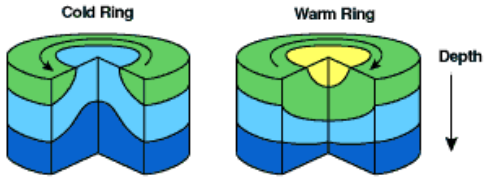

Figure 5.1: Cold core and warm core rings[4]

As eddies can transport huge water masses with particular properties like as being e.g. very salty or just warmer than the surrounding ocean, over long distances, they are of great importance to the global climate. The Agulhas rings e.g. transport warm and salty water from the Agulhas current into the Atlantic, consequently influencing the Gulf stream and hence even the climate in the northern latitudes. As more and more warm and salty water is transported into the Atlantic due to these rings, the effect on the Gulf stream is constantly intensifying as shown in ScienceDaily (2008). Beside this also the biological impact of ocean eddies cannot be neglected, as they carry huge quantities of nutrients (Lehahn et al., 2011). Until now meso-scale processes could barely be seen in satellite gravity data as the spatial and temporal resolution of the current gravity missions have been too coarse. The detection of eddy variability, however, is one of the efforts of future satellite gravity missions. Because of their characteristics eddies can be seen in various fields, such as temperature-, salinity- or SSH-fields. Consequently the use of satellite altimeter data is an useful tool to detect eddy variability. Anyway, the spatial resolution is also limited here, hence not all ocean eddies can be resolved as well. The ability of climate models to resolve eddies is for sure restricted to their grid resolution. Table 5.1 gives a

[3] `http://www.gfdl.noaa.gov/ocean-mesoscale-eddies`, accessed 2015/06

[4] Source:`http://disc.sci.gsfc.nasa.gov/education-and-outreach/additional/science-focus/classic_scenes/07_classics_rings.shtml`, accessed 2015/08

short overview on the various climate models and their opportunities to resolve eddies.

Table 5.1: Ocean models classified on their possibility to resolve eddies

climate model	grid resolution [°]	spatial resolution [km]	visability
OMCT	1	100	non-eddy resolving
ORCA025	0.25	30	eddy permitting
MPIOM	0.1	12	eddy resolving

It might seem a little irritating, that an ocean model with a spatial resolution of 100 km is classified as *non-eddy resolving*, though the the spatial resolution would very well fit with the average diameter of meso-scale eddies. This, however is due to the principle formation process of eddies through baroclinic instability which usually occurs at very small scales (<20 km).

5.1.3 Baroclinic and barotropic instability

As mentioned in the previous section, eddies are mainly formed through dynamical instabilities. This can either be through baroclinic or barotropic instability. To understand these dynamical processes, the terms of baroclinic and barotropic have to be discussed first. An ocean current can basically be split up into a barotropic and a baroclinic mode. Barotropic refers to the property of an ocean current being depth-independent, meaning that a barotropic current is not changing its direction or speed with depth, having the same velocity from the bottom to the surface. The barotropic mode is linked to the sea surface height, areas of constant pressure and areas of constant density are always parallel to the sea surface. Whereas a baroclinic current is depth-dependent and hence is changing its direction and speed with depth. Rewording, the term baroclinic defines that isobars (areas of constant pressure) and isotherms (areas of constant temperature) are not parallel (as they are for a barotropic ocean), but cross each other, leading to the existence of a temperature gradient. Figure 5.2 visualizes a baroclinic and a barotropic ocean. As it can be very well seen in this figure, the barotropic mode is directly linked to the sea surface height. This does however not account for the baroclinic mode.

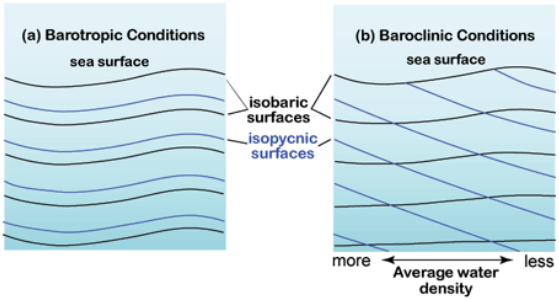

Figure 5.2: Barotropic and baroclinic conditions in the ocean[5]

[5]Source: `http://www.oc.nps.edu/nom/day1/partb.html`, accessed 2015/07

Instabilities can arise in a baroclinic as well as in a barotropic stratified ocean due to disorders, called barotropic resp. baroclinic instability. Baroclinic instability occurs due to vertical shear, till example through existance of a very large temperature gradient. This causes turbulences that avail the potential energy of the stratified current to create meso-scale eddies. Baroclinic instability usually occurs on very small scales, which makes it very hard for ocean models to account for this dynamical process (CIESM, 2005). Hence the modeling of eddies formed by baroclinic instability is not always adequately possible.

The barotropic instability mainly occurs in western boundary currents and around the equator due to horizontal shear and also causes meso-scale eddies to emerge. As the barotropic fraction of the flux is basically having very high velocities (compared to the lower velocities of the baroclinic part) it hence has large kinetic energy as well. This kinetic energy of the mean flux is then used by turbulences, again leading to high-energetic meso-scale ocean eddies. Further information on this topic can be found in (Colling et al., 2001) or (Drakos, 1994).

5.2 Regions with meso-scale eddy variability

Several regions with meso-scale variability can be found throughout the ocean, e.g. in the region of the Gulf current or the Kurushio current in the Pacific, however, in this thesis it will be focused on two particular areas of interests in the Atlantic ocean, the Cape Basin on the one hand and the Argentine Basin on the other hand. The locations of the selected observation areas are depicted in figure 5.3 and a detailed view of the basins is given in figure 5.4.

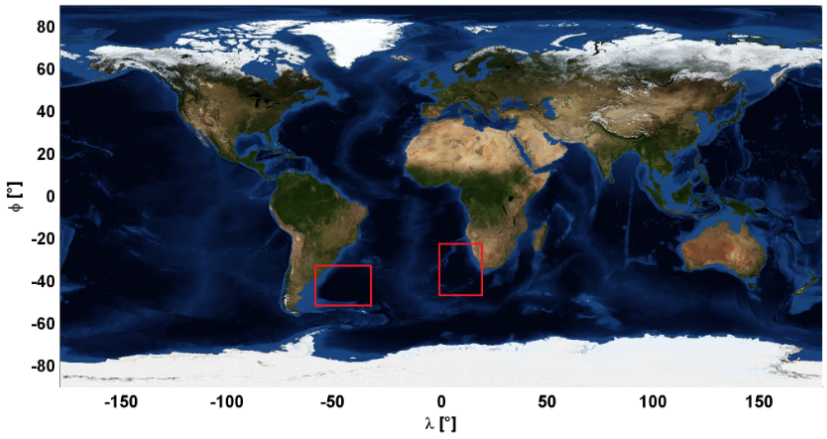

Figure 5.3: Observation areas

5.2.1 Cape Basin

One region that shows a significant meso-scale activity is the area south-west of the South African coastline, called Cape Basin. The Cape Basin extends around 1500 km in the north-south direction and almost 1000 km in east-west direction and spans the area around

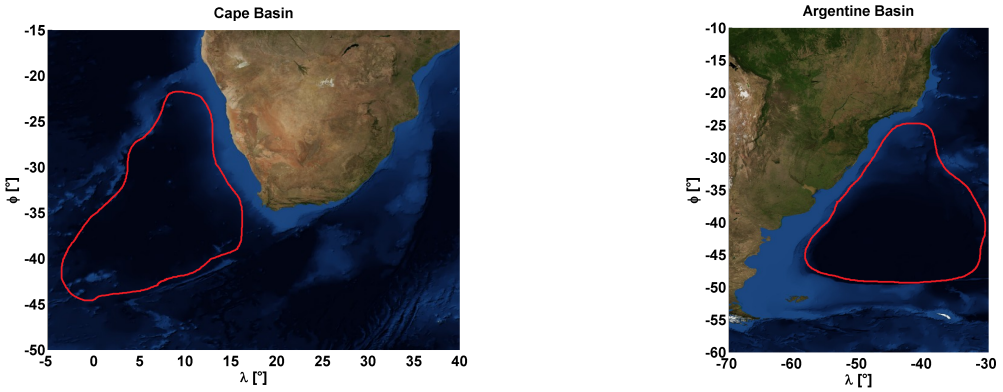

(a) Cape Basin

(b) Argentine Basin

Figure 5.4: Detailed view of Cape Basin and Argentine Basin

35°S and 6°E. This area has been a target of numerous research projects for years now, as the retroflection of the Agulhas current is not complete, leading to a conveyance of warm and salty water from the Indian ocean into the Atlantic ocean as a part of the global termohaline circulation. This phenomena is called *Agulhas Leakage* and exists due to the formation of multitudinous high energetic ocean eddies in the retroflection zone of the Agulhas current. The emergence of those eddies is mainly in the region between 15°E - 20°E and 38°S - 42°S, whereby the ocean sea floor properties are prevailing for their formation process (Dencausse et al., 2010). Both cyclonic and anticyclonic eddies originate in this region, where the cyclonic eddies are usually of larger diameter (200-300 km) as the anticyclonic eddies (100 km). The progress of the eddies is diverging, a few cross the Walvis Ridge in the northern direction, but most of them flow westwards shortly ahead of the Walvis ridge. The majority of the cyclonic eddies however never leaves the Cape Basin as it vanishes beforehand. The average duration of life of Agulhas rings lies around 3 months, some having an even lower life expectancy of only a few weeks (Dencausse et al., 2010).

5.2.2 Argentine Basin

Another region noted for a high meso-scale ocean eddy occurrence is the Argentine Basin (see figure 5.4 (b)). This basin is situated off the coast of the Argentine mainland and reaches a depth of almost 6 km at its deepest point. The basin is well known for its turbulences, as two currents, the cold Malvina current, which branches from the ACC (Antarctic Circumpolar Current) and the warm Brazil current encounter each other in this basin. This very complex dynamical region is called the Brazil - Malvina - Confluence zone. Because of the two completely contrary currents colliding, immense temperature- and salinity gradients are generated in this area, leading to baroclinic instability and consequently to the formation of eddies. A simultaneous occurrence of several meso-scale eddies is possible in this region. Another well known feature in the Argentine Basin is the so called Zapiola drift, a barotropic anticyclonic current around the undersea mountain Zapiola Rise situated at 44°S and 45°W. This huge anticyclonic drift is said to be driven by eddies in the confluence zone (de Miranda et al., 1999).

6 OBP variability from GRACE and ESA ESM

As the goal of this thesis is to provide a statement on the needed improvement in accuracy of future satellite gravity missions in order to detect meso-scale variability in the ocean, investigations on modeled data and actual gravity field data have been made in the interest of determining similarities and disparities to demonstrate the current possibilities of gravity field missions. The following chapter will give an insight into those possibilities but also on the prevailing limitations, both on global and regional scale. The comparison of the simulated and the gravity field data is primarily based on RMS variability, but also the examination of EOF pattern and degree variances has been taken into account.

6.1 Global

Starting at global scale, maps of gridded RMS values have been created. The same data as for the evaluation of the eustatic sea-level rise has been used (ITSG-Grace2014 gravity field solution and ESA ESM O component). Hence the same preliminary actions had to be executed for the GRACE data set, such as the reduction of the static solution in order to gain the time-dependent gravity field, the replacement of the GRACE C20 and degree 1 coefficients (geocenter motion), the removal of the GIA and the applied filter method for the smoothing of the GRACE stripes. The AOD1B component *oba* (from d/o=1) has also been added back to the GRACE monthly means to receive the full ocean signal. For a better comparability the time period from 2004 to 2006 has been chosen, as both data sets are overlapping during this time span. Figure 6.1 shows the global RMS values over all ocean areas up to a maximum degree of 60 for both the GRACE and the simulated data from the ESA ESM.

Although the ITSG-Grace2014 solution has been smoothed with a 500 km Gaussian filter radius, there are still slight north-south stripes visible, especially in regions close to the equator, as it can be seen in figure 6.1 (a). Yet there is already a strong accordance between both figures 6.1 (a) and (b) regarding the most significant RMS values. Both the GRACE data as well as the data from the oceanic component of the updated ESA ESM show high ocean bottom pressure variability in the area of the antarctic circumpolar current (ACC) and in the northern Pacific Ocean. While the model reaches variability far $>$ 5 hPa in certain areas, the variations in the GRACE field are lower with around 3 - 4 hPa. Beside this, also the effect of land leakage due to Gaussian filtering can be observed very well in coastal areas (especially Greenland and South-East Asia) in the GRACE data (figure 6.1 (a)).

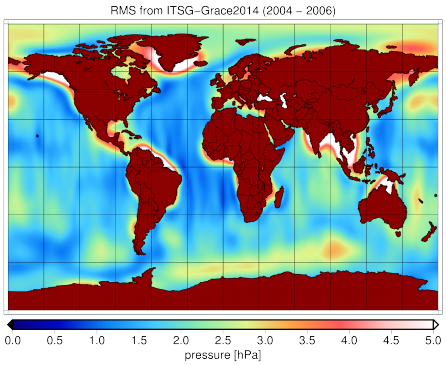

(a) Global RMS of OBP anomalies (d/o = 60) from ITSG-Grace2014 smoothed with a 500 km Gaussian filter radius

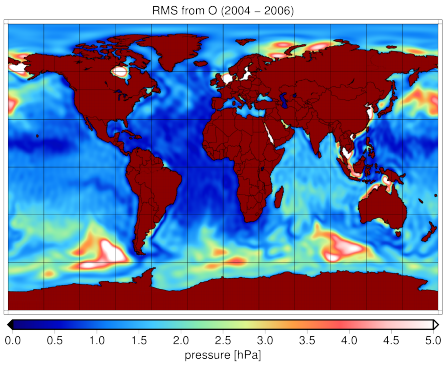

(b) Global RMS of OBP anomalies (d/o = 60) from ESA ESM O (unfiltered)

Figure 6.1: RMS values of global OBP anomalies over the period 2004 - 2006

Figure 6.2 depicts the RMS values of the ITSG-Grace2014 solution, but without the de-aliasing component *oba* added back. Ignoring the mandatory addition of the AOD1B de-aliasing component *oba*, the time-variable GRACE field should not show any variations in the ocean. Nevertheless, figure 6.2 indicates variability of up to 2.5 hPa, especially in the Argentine Basin, the region around Cape Agulhas and the ACC. This points to the fact that oceanic processes in these areas are insufficiently modeled by the de-aliasing background model OMCT. Those regions are known for their meso-scale activity and like mentioned in the previous chapter, the modeling of their formation sources, the dynamical instabilities, requires a high-resolution model, which the OMCT is not.

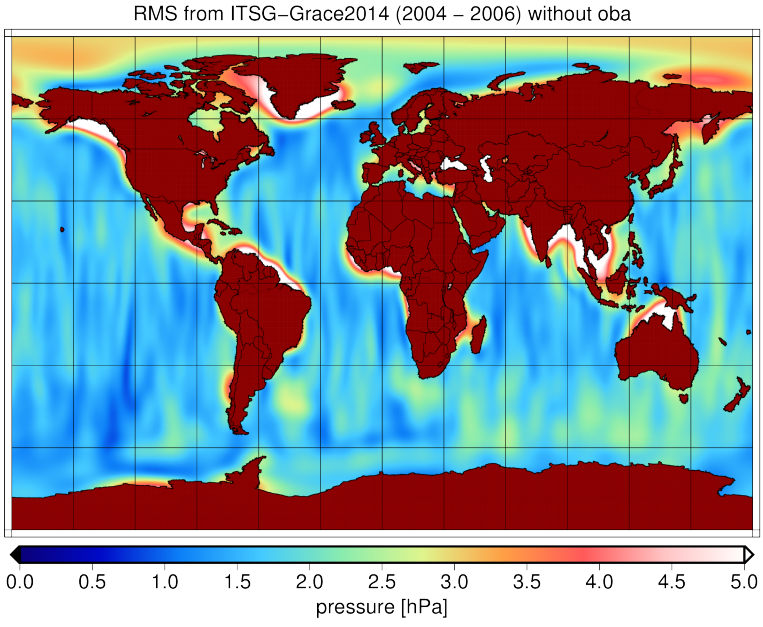

Figure 6.2: RMS values of global OBP anomalies from ITSG-Grace2014 until d/o=60 smoothed with a 500 km Gaussian filter radius without the AOD1B oba component added back

The contribution of neglecting those processes in the de-aliasing model to the total error budget is though low (Dobslaw et al., 2015) and a necessity of modeling them is not given for the current achievable accuracy of GRACE. However, aiming to improve the possibilities of GRACE in detecting meso-scale variability, the addition of those processes to the de-aliasing model might be necessary in order to reach the required accuracy.

Figure 6.3 demonstrates the differences between the various background models of the updated ESA ESM. Taking a closer look at the oceanic component of the updated ESA ESM in figure 6.3 (a), it can be seen that no meso-scale variability in the Argentine Basin and the Cape Basin is visible so far. However, increasing the depicted degree to 120, those meso-scale OBP variations become apparent as now the background model of the ESM is the high-resolutional MPIOM. Beside the variability in the Argentine and the Cape Basin, also variations in the western part of the northern Atlantic can be seen, indicating meso-scale activity in the region of the Gulf current.

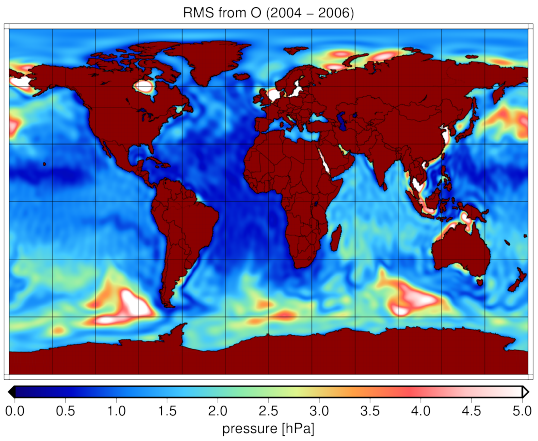

(a) Global RMS of OBP anomalies (d/o = 60) from ESA ESM O over the period 2004 - 2006

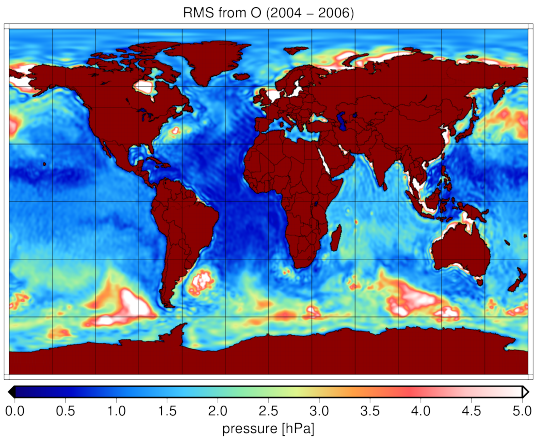

(b) Global RMS of OBP anomalies (d/o = 120) from ESA ESM O over the period 2004 - 2006

Figure 6.3: RMS values of global OBP anomalies from the ESA ESM O component

6.2 Regional

In the further course of the investigations on the current possibilities of satellite gravity missions to detect meso-scale activities in the ocean, the focus will lie on the OBP variability in the southern Atlantic regions of the Argentine Basin and the Cape Basin. For detailed information on the present state of knowledge on the ocean activities in these regions see section 5.2.1. Concerning the used data the same assumptions as for the global analysis pertain. The investigations were structured as follows. Beginning with the Argentine Basin, the effect of the application of Gaussian filter with different radii has been examined. Further the temporal progress of the OBP variations in the basin as well as at distinctly selected observation points has been studied and compared, followed by a spatial analysis using EOF decomposition.

6.2.1 Argentine Basin

Starting with the region of the Argentine Basin, an almost 6000 m deep basin off the coast of the South American mainland, that is known for its high kinetic eddy energy, the observation area has been limited to 35°W - 70°W and 30°S - 55°S. It is known that the meso-scale variability in this basin takes up a region of almost 1000 kilometers in diameter.

First of all, the effect of different Gaussian filter radii has been tested in order to ascertain whether resp. when the signal usually hidden beneath the GRACE systematic errors starts to appear. As mass signals in the ocean are far smaller than on continental areas, it is expected that a comparatively large filter radius has to be applied to the data. Since a filter is mandatory for the GRACE data to reduce the stripes, the modeled data has to be filtered as well to insure the comparability of both data sets as the same conditions have to be held in order to postulate a meaningful statement.

Figure 6.4 (GRACE) and figure 6.5 (ESA ESM O) reveal the impact of the various Gaussian filter radii applied, both in terms of RMS values computed over a period of 2004-2006. The scale limits of the figures have been chosen in a way such that the most important changes during the application of the Gaussian filter can easily be observed. This unfortunately results in white figures for the first utilized filter radii as the values are much higher there, though not meaningful. It can easily be seen that the noise in the GRACE data starts to abate first at a filter radius of 400 km, at a filter radius of 500 km a significant signal starts to appear. For the ESA ESM data in return a signal is already visible at a Gaussian filter radius of 100 km, however just a very inconspicuous one. An expected meso-scale variability is though not apparent so far due to the low maximum degree of 60. Therefore the same procedure has been applied to the data up to degree 120, visualized in figure 6.6 and 6.7.

Now the ESA ESM reveals a signal of up to 7 hPa at the western boundary of the basin, in the so called Malvina-Brazil-Confluence Zone. Applying a Gaussian filter radius of 100 km, a part of the signal remains present, but is significantly diminished in signal strength. From the usage of a Gaussian filter radius of 200 km however the significant meso-scale variability vanishes completely. The results for the GRACE data in contrast do not change greatly like expected. GRACE is in contrast to the model seeing a wide more large-scaled variability situated in the center of the basin. The variations simulated by the ESA ESM are most likely due to eddy activity in the highly dynamical region of the Malvina-Brazil-Confluence zone and seem far too small to be adequately resolved by GRACE. Having averaged diameters of around 100 km, the spatial resolution of GRACE is yet not sufficient, especially because of the compulsory use of a Gaussian filter with minimum radius of 500 km. At this stage it has to be pointed out that a depiction of GRACE data with a maximum cut off degree of 120 in combination with a Gaussian filter radius > 200 is generally not meaningful due to the characteristics of the Gaussian filter. The just presented figures showed that a minimum Gaussian filter radius of 500 km is mandatory in order to detect significant signal content, which diminishes the depicted degree to 40. This makes the use of a gravity field solution with maximum degree 120 generally pointless. Nevertheless it has been used here for the purpose of comparison.

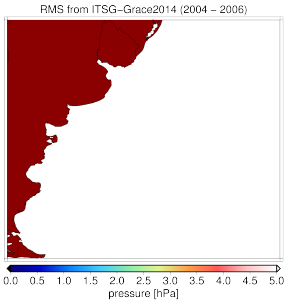

(a) 0 km Gaussian filtered

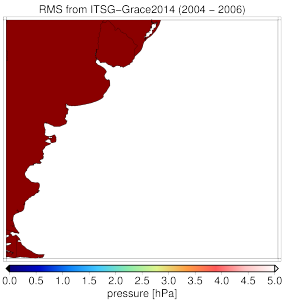

(b) 100 km Gaussian filtered

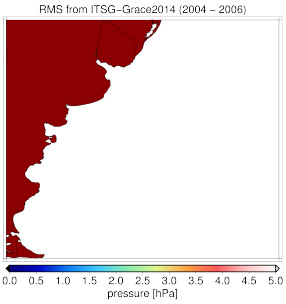

(c) 200 km Gaussian filtered

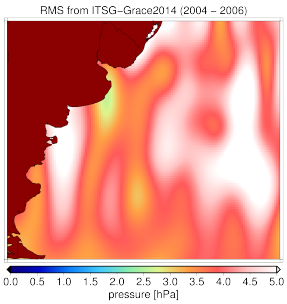

(d) 300 km Gaussian filtered

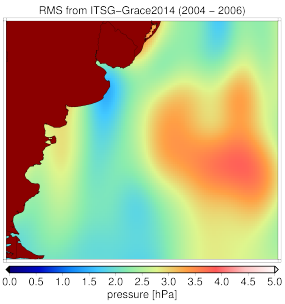

(e) 400 km Gaussian filtered

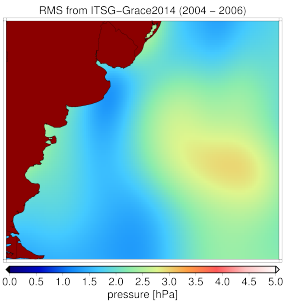

(f) 500 km Gaussian filtered

Figure 6.4: RMS variability of GRACE OBP anomalies filtered with different Gaussian radii until d/o = 60 in the Argentine Basin

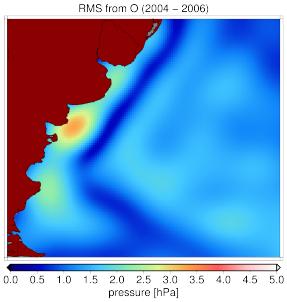

(a) 0 km Gaussian filtered

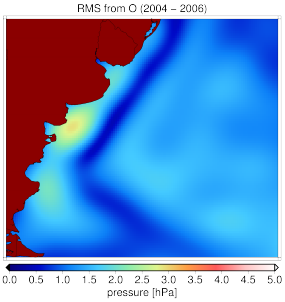

(b) 100 km Gaussian filtered

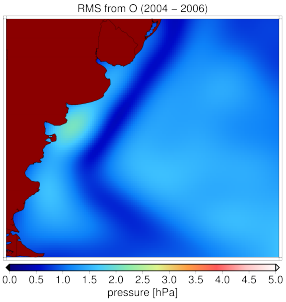

(c) 200 km Gaussian filtered

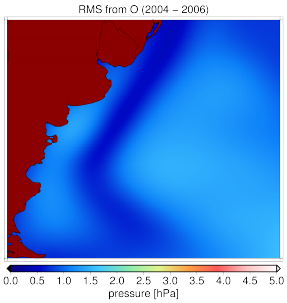

(d) 300 km Gaussian filtered

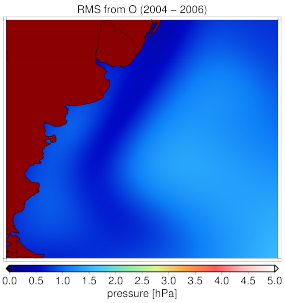

(e) 400 km Gaussian filtered

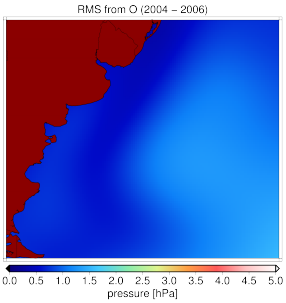

(f) 500 km Gaussian filtered

Figure 6.5: RMS variability of ESA ESM OBP anomalies filtered with different Gaussian radii until d/o = 60 in the Argentine Basin

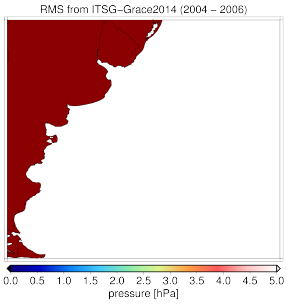

(a) 0 km Gaussian filtered

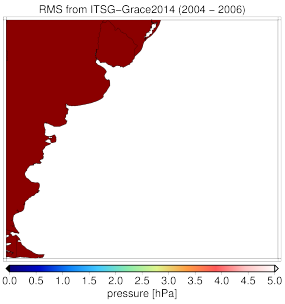

(b) 100 km Gaussian filtered

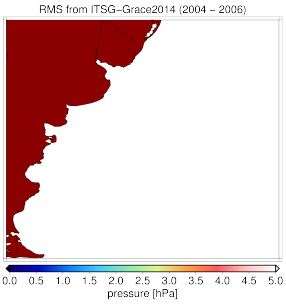

(c) 200 km Gaussian filtered

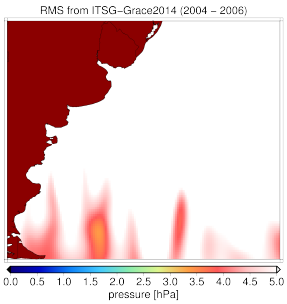

(d) 300 km Gaussian filtered

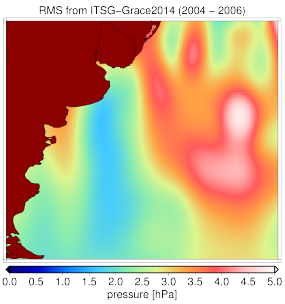

(e) 400 km Gaussian filtered

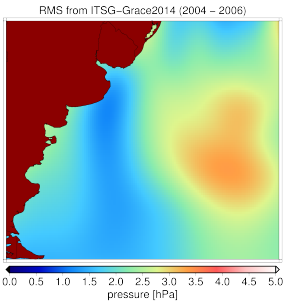

(f) 500 km Gaussian filtered

Figure 6.6: RMS variability of GRACE OBP anomalies filtered with different Gaussian radii until d/o = 120 in the Argentine Basin

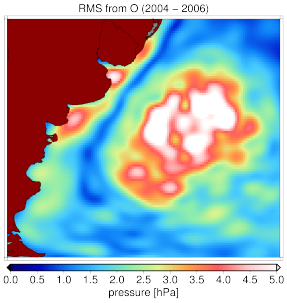

(a) 0 km Gaussian filtered

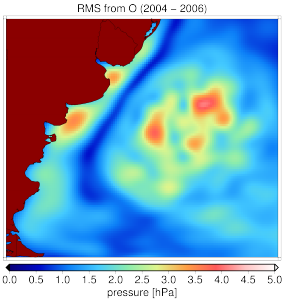

(b) 100 km Gaussian filtered

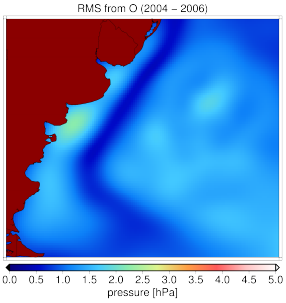

(c) 200 km Gaussian filtered

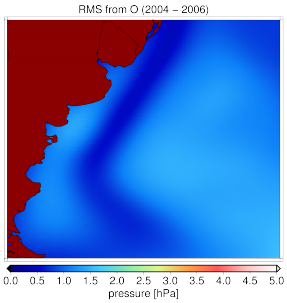

(d) 300 km Gaussian filtered

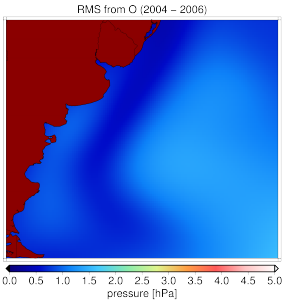

(e) 400 km Gaussian filtered

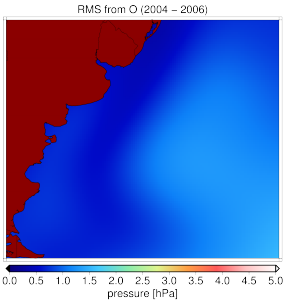

(f) 500 km Gaussian filtered

Figure 6.7: RMS variability of ESA ESM OBP anomalies filtered with different Gaussian radii until d/o = 120 in the Argentine Basin

The difficulty in comparing the GRACE data with the simulated data of the ESA ESM is on the one hand side the just mentioned fact that the GRACE data has to be filtered in order to detect a geophysical signal. For the complete comparability of the data sets, the ESA ESM data has to be filtered as well. As shown in the previous figures, an applied filter on the ESA ESM O component causes the meso-scale variability to vanish quite quickly. On the other hand side, the simulated meso-scale variations are basically represented by higher degree coefficients. As the high-resolution MPIOM is used for the spherical harmonics in the ESA ESM from degree 61 to 180, at least a degree of 70 is needed to depict these activities. Because of the fact that the gravity field solution should be examined on the detectability of meso-scale activities a maximum degree of 120 is occasionally used in further investigations. Because of the previously mentioned facts it has to be pointed out that this is consciously chosen only for the reason of comparability.

Comparison of daily solutions

Beside the study of monthly solutions, also data based on daily means has been tested and compared, as meso-scale ocean eddies are sometimes having a life expectancy of only a few weeks. Hence, these eddies would not be able to be adequately resolved in monthly averaged data. As the maximum degree of the kalman smoothed daily ITSG-Grace2014 solutions is 40, also the maximum degree of the evaluated updated ESA ESM O component has been reduced to 40 here, corresponding to a spatial resolution of 500 km. An additional filtering of the GRACE data is not needed here, as an adequate filter has already been applied during the processing of the daily solution.

As expected the meso-scale variability is no longer visible in the ESA ESM computed RMS values (see figure 6.8 (b)) based on daily means. Basically RMS variations based on the daily solutions assort very well with each other. This very good accordance is highly probable due to the use of the OMCT in the processing of the daily ITSG-Grace2014 solution. With variations over 5 hPa the signal is though stronger for the GRACE results (figure 6.8 (a)) as for the modeled results, showing that there might exist a stronger signal than the model comprises. To compare the results of the daily solutions directly with those of the monthly solutions, figure 6.8 (c), (d) and (e) illustrate the RMS variability derived from the monthly averaged data.

The most intense signal observable in the gravity field solutions, both daily and monthly, is present in the same area and possibly defines the so-called Zapiola Anticyclone, a huge barotropic stationary anticyclone (Saunders and King, 1995) rotating around the underwater mountain Zapiola Rise, located at 45W and 44S. Having an extent of around 1000 km zonally and 300 km meridionally it is likely that the GRACE derived OBP variations in figure 6.8 (a) and (c) are referred to this phenomenon. The Zapiola Anticyclone is said to be of strong barotropic character, strengthening the assumption that the model is underrating this variability as the signal is generally stronger for the GRACE results. (de Miranda et al., 1999) states, that the anticyclone is said to be driven through meso-scale eddy variability in the western boundary of the basin. The variability visible in the results from the ESA ESM (figure 6.8 (e)) is primarily reflecting this meso-scale induced signal. The made examinations lead to a first presumption that GRACE is currently not able to detect meso-scale variability in the Argentine Basin.

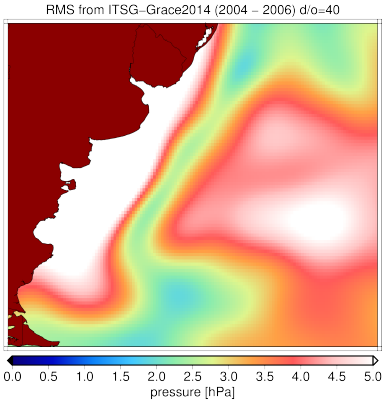

(a) RMS values based on daily ITSG-Grace2014 solution

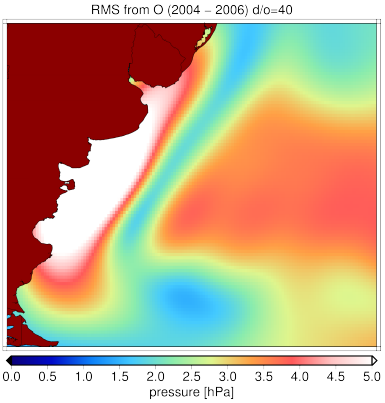

(b) RMS values based on daily solution ESA ESM

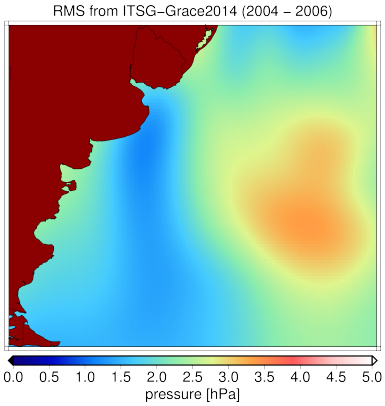

(c) RMS values based on monthly solution ITSG-Grace2014 (500 km Gaussian filtered)

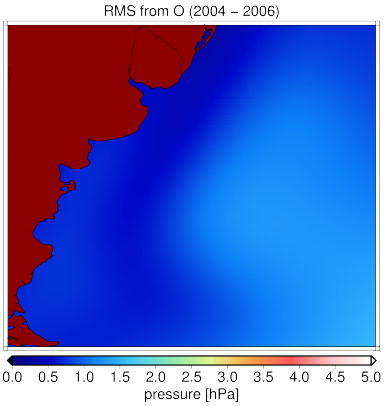

(d) RMS values based on monthly solution ESA ESM (500 km Gaussian filtered)

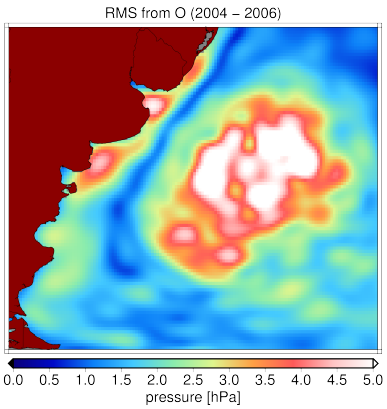

(e) RMS values based on monthly solution ESA ESM (unfiltered)

Figure 6.8: RMS variability derived from ESA ESM and GRACE over the period 2004 - 2006

Temporal analysis

For further examinations of the gravity field data and the model data on their correlation concerning present signals, the time series of OBP variability in the Argentine Basin have been studied. First, the basin-averaged OBP anomalies have been determined for the period of January 2004 to December 2006 both for the daily and the monthly averaged data, shown in figure 6.9. The time series of the daily means (based on a maximum degree of 40) show a very good accordance, having a correlation factor of 87%. Recalling the great conformity of the RMS values derived from daily averages, this is not surprising. This is due to the circumstance that the OMCT is used in the regularization during the processing of the daily solutions. This leads to an adaptation of the daily solutions to the OMCT. The correlation of the basin-averaged OBP variations based on the monthly means (both filtered with a 500 km Gaussian filter and a maximum degree of 120) is with 52% essentially lower, originating from the characteristics of the generation of monthly means as well as the fact that the OMCT is not affecting the monthly GRACE solutions. Although the OMCT has been used in the de-aliasing model during GRACE processing, the back-addition in the post-processing removes the influence of the model (Dobslaw, 2007).

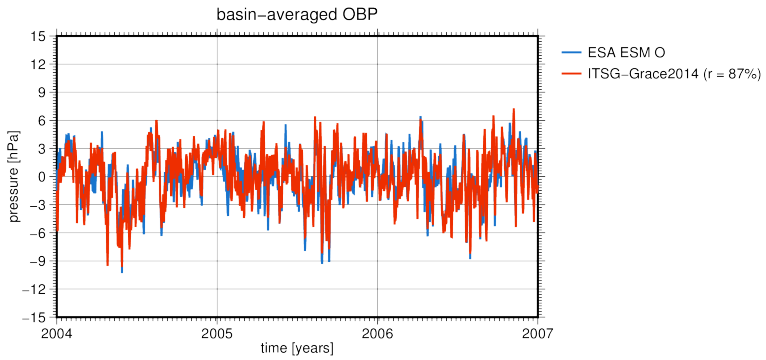

(a) Basin-averaged OBP based on daily means

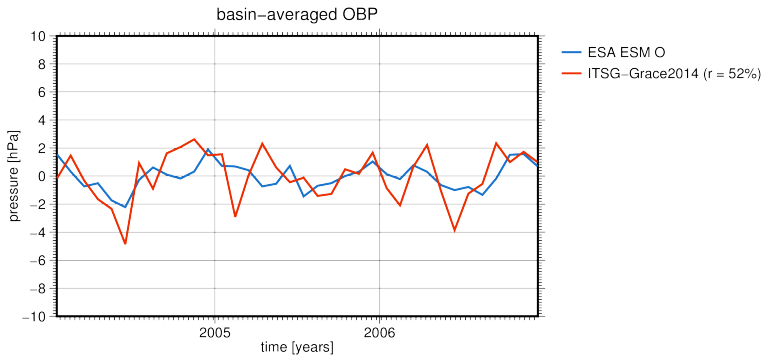

(b) Basin-averaged OBP based on monthly means

Figure 6.9: Time series of basin-averaged OBP in Argentine Basin over the period of 01-2004 to 12-2006 (a) based on the daily averaged data with maximum degree 40 and (b) based on the monthly averaged data with maximum degree of 120 with 500 km Gaussian filter applied

Furthermore, OBP time series at three different observation points in the Argentine Basin have been observed, comparing the two data sets for similarities and differences. The observation points have been chosen in such way that two points lie in the region of high meso-scale activity in the western boundary of the basin and one close to the so-called Zapiola Rise. In figure 6.10 the location of the observation points as well as the Zapiola Rise are depicted.

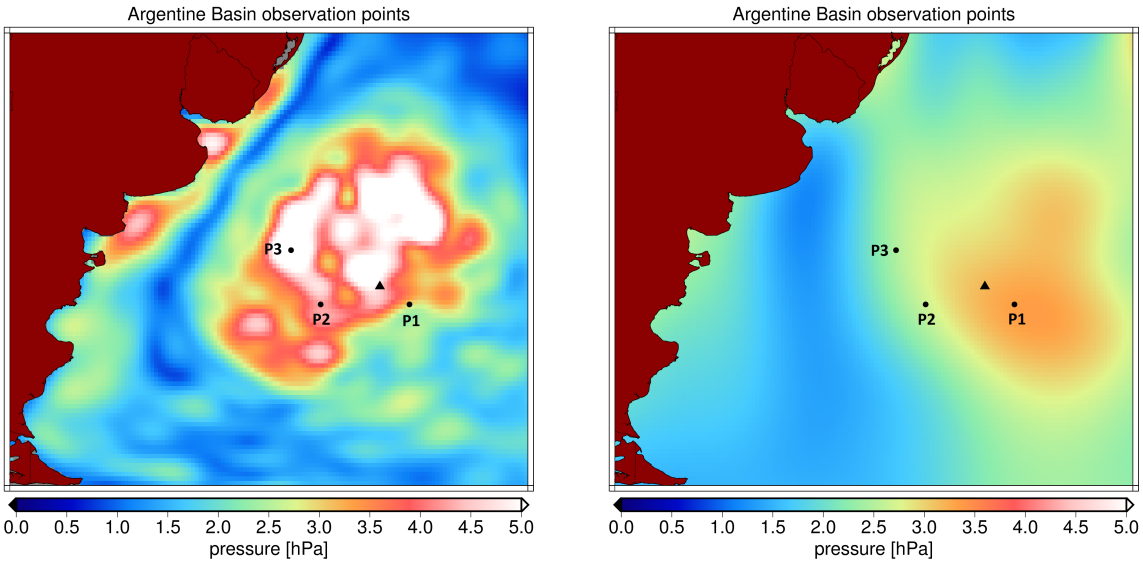

(a) Location of observation points on the background of RMS values of monthly ESA ESM O component (d/o=120) unfiltered

(b) Location of observation points on the background of RMS values of monthly ITSG-Grace2014 solution (d/o=120) filtered with 500 km Gaussian filter

Figure 6.10: Location of observation points (marked with dots) and the undersea mountain Zapiola Rise (marked with a triangle)

Because of the difficulties in comparing the various data sets, described in the previous section, three different comprises have been made for the temporal analysis of OBP variability at the selected locations:

1. First the 500 km Gaussian filtered OBP anomalies from the monthly ITSG-Grace2014 solution have been compared to the unfiltered OBP anoamlies from the monthly averaged ESA ESM O component, both at a maximum degree of 120.

2. Secondly the OBP anomalies from both the monthly ITSG-Grace2014 solution and the monthly averaged ESA ESM O component have been filtered with a 500 km Gaussian filter, again at a maximum degree of 120.

3. Last, the OBP anomalies of the daily solutions have been compared at a maximum degree of 40.

The first comparison method shall reveal how far the GRACE data can resolve the meso-scale activity. The second one is made in order to show the resemblance between the gravity field data and the model data without any meso-scale activity simulated. The

third method should then demonstrate the difference between the monthly and the daily averaged data sets.

Figure 6.11 depicts the first comparison method, in which the Gaussian filter has only been applied to the GRACE data. This method is only done for the reason to illustrate the different sources of OBP signals of the various data sets. A degree of 120 has again been taken only for the sake of comparability. Looking at the figure 6.11 it gets obvious that GRACE is not seeing meso-scale activities, as the correlation of the observed time series gets lower and lower with the location of the points being more in the western boundary region of the basin. Starting with a correlation of 29% near the Zapiola Rise, it decreases to 6% when going to the west and is at its lowest with only -1% in the western boundary of the region with known meso-scale variations. Comparing the progress and the amplitudes of the time series, it can also be seen that the amplitude of the ESA ESM time series is generally much higher at the points in the western boundary of the basin, whereas at the observation point close to the Zapiola Rise the GRACE time series shows more significant amplitudes. Beside this, a slight seasonality (of around 5 months) is detectable in the GRACE time series (see figure 6.11 (a)) as well.

Figure 6.12 illustrates the temporal progress of the filtered OBP anomalies. Here the time series of the OBP anomalies from the ESA ESM is completely smoothed, not showing any special activities but only a slight annual cycle at all three observation points. The correlation results are better for point 2 (49°W 45°S) and point 3 (51°W 42°S) compared to the first method, as the meso-scale variability has disappeared due to the strong filtering.

The time series based on daily scales are illustrated in figure 6.13. The correlation results on the basis of the daily means are unsurprisingly much better, for the same reasons like explained when interpreting the basin-averaged time series. No real difference is seen between the three observation points, all having a correlation coefficient of around 80%.

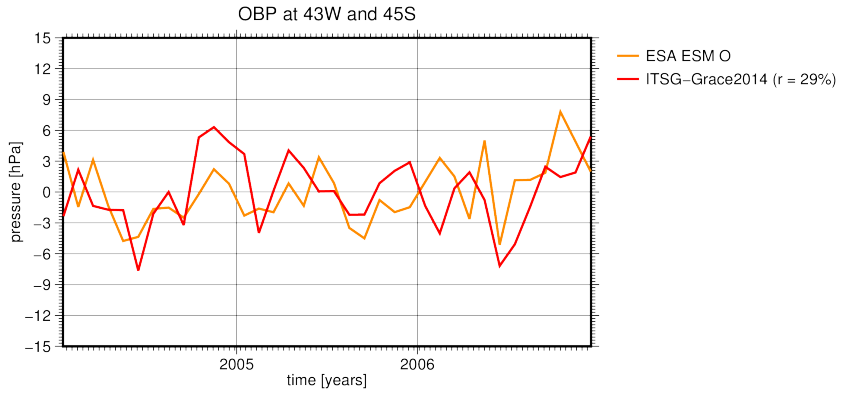

(a) OBP variations at 43W and 45S

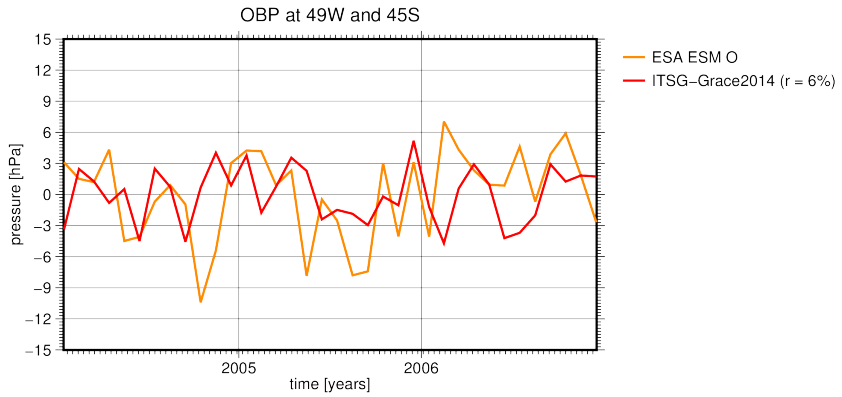

(b) OBP variations at 49W and 45S

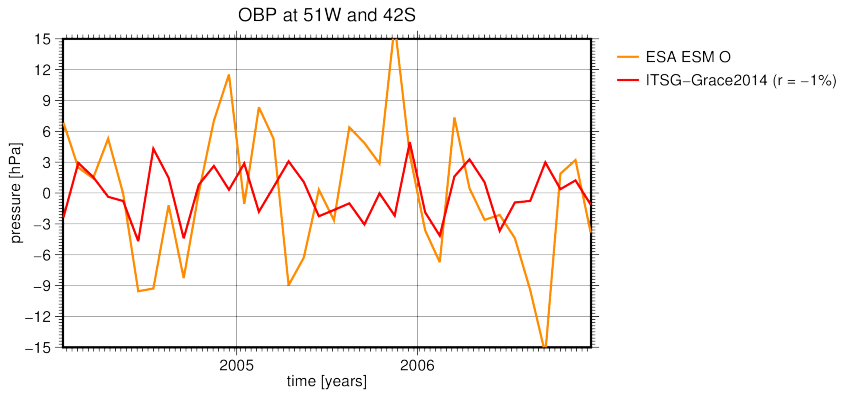

(c) OBP variations at 51W and 42S

Figure 6.11: OBP variations from monthly ITSG-Grace2014 solution (500 km Gaussian filtered) and monthly averaged ESA ESM (unfiltered) at different observation points

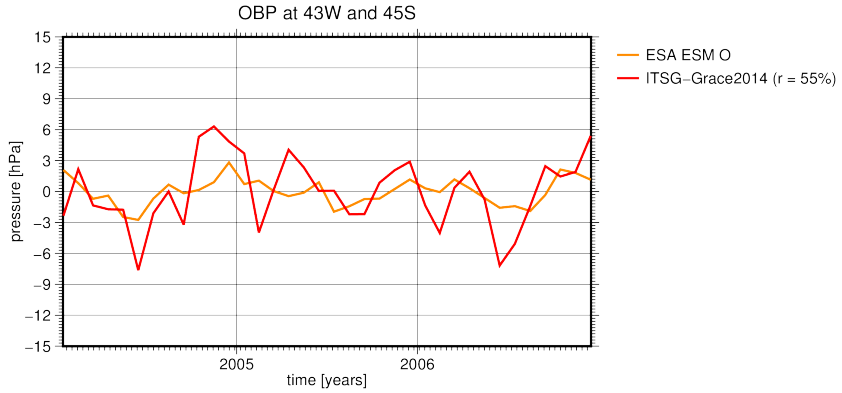

(a) OBP variations at 43W and 45S

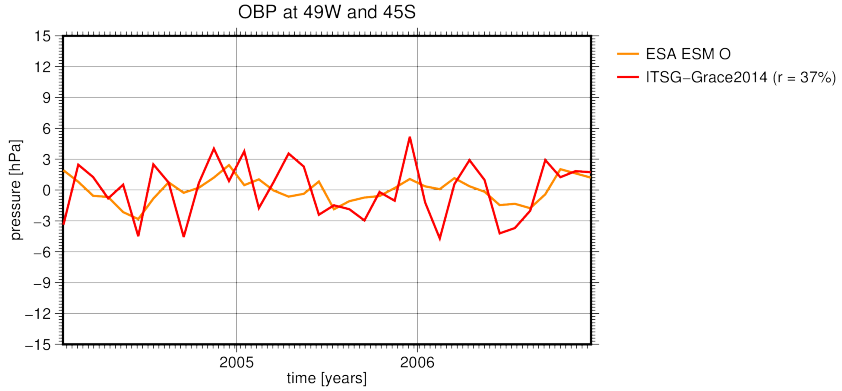

(b) OBP variations at 49W and 45S

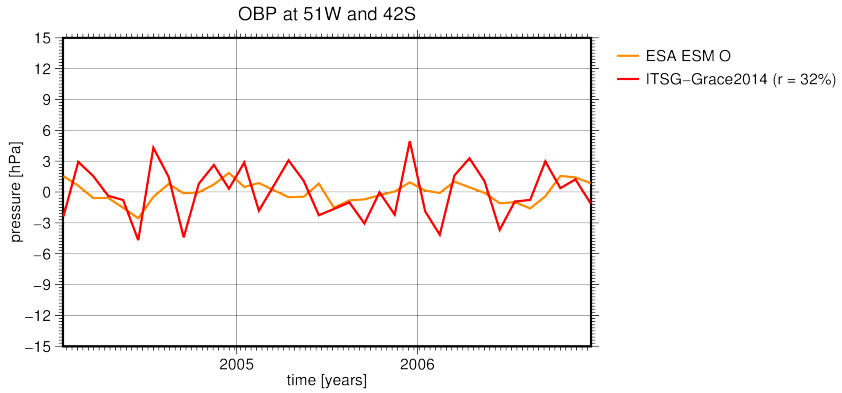

(c) OBP variations at 51W and 42S

Figure 6.12: OBP variations from monthly ITSG-Grace2014 solution and monthly averaged ESA ESM (both with a 500 km Gaussian filter applied) at different observation points

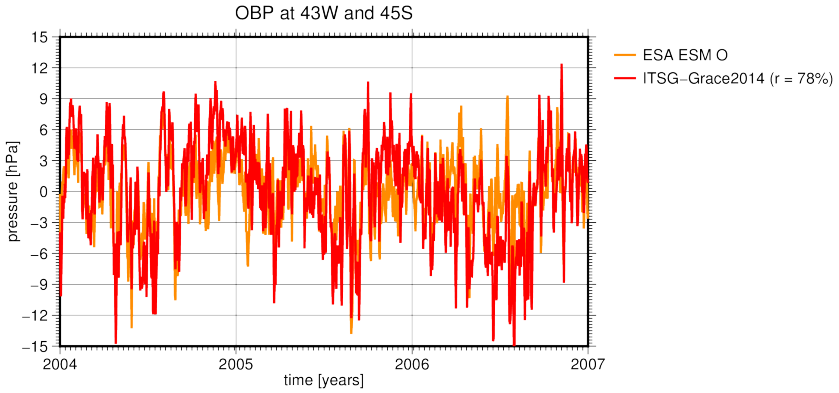

(a) OBP variations at 43W and 45S

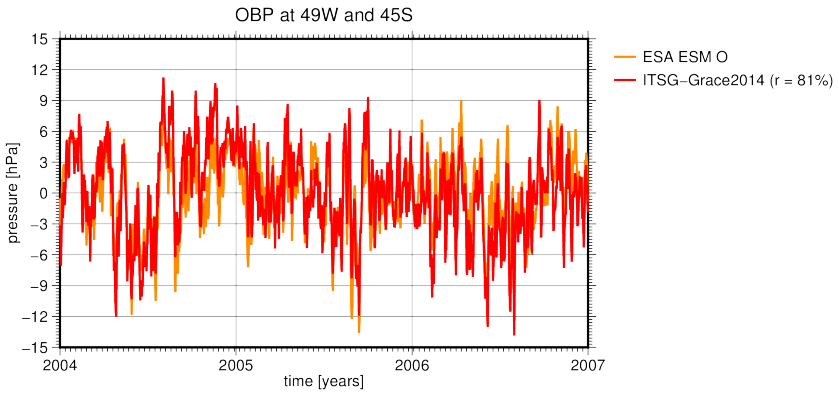

(b) OBP variations at 49W and 45S

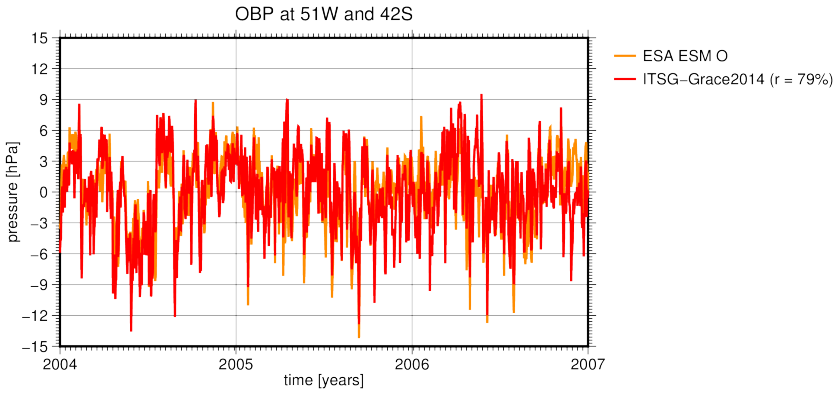

(c) OBP variations at 51W and 42S

Figure 6.13: OBP variations from daily ITSG-Grace2014 solution and daily averaged ESA ESM at different observation points

Spatial patterns

Beside the investigations of the temporal process of the OBP anomalies, also the spatial patterns of the signals have been examined in order to detect the sources of the present OBP anomalies. As EOF decomposition is usually better done for longer time series, the periods 1995 - 2006 for the ESA ESM and 2003 - 2013 for GRACE have been taken. Basically it has to be pointed out that the interpretation of EOF modes in terms of underlying geophysical signals has to be done with caution (Dommenget and Latif, 2002). The EOF decomposition is a merely statistical tool and the property of the EOF patterns being orthogonal (EOF modes of higher modes are constrained to be orthogonal to the first one) does not always coincide with the real nature of geophysical signals. The opinions about handling the EOF analysis as tool to prove the underlying physics of the variability are widespread. (Monahan et al., 2009) even states that EOF modes shall generally not be interpreted individually. Furthermore the determination of the dominant modes is not distinctly specified. Several methods exist for the purpose of determining the modes that contain important information, however, the yielded results differ widely from each other. The so-called *Cattell scree Test* (Cattell, 1966), which is only based on a visual reflection, is one of them. It is sometimes also referred to as the *elbow test*, as the way to find the modes with significant information content is to detect a considerable decrease, which mostly results in an elbow. The one mode marking the start of the elbow will be the last one taken into account. Figure 6.14 is a so-called scree plot, depicting the explained variances of the EOF modes in decreasing order.

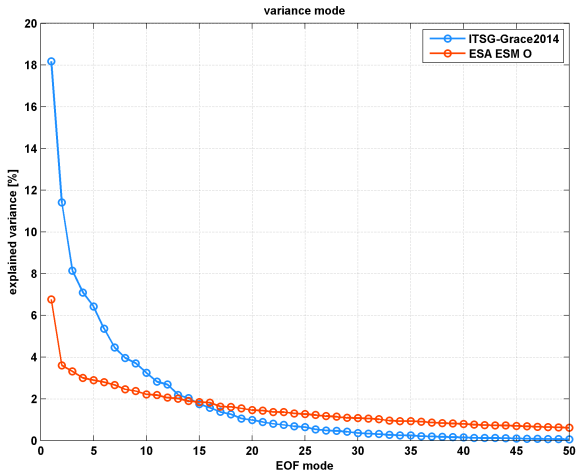

Figure 6.14: Comparison of explained variances (Argentine Basin)

A look at the figure reveals the difficulty of this method. For the ESA ESM derived modes the elbow is easy to detect, the GRACE derived curve however has a less plunging characteristics, consequently the determination of the last significant mode is quite arbitrary. Using this criterion 2 modes would be selected for the ESA ESM and 8 for the GRACE data. Another criterion is the *90% criterion*, which advises to take all modes into account that together explain 90% of the total variance. This criterion yields 76 representative modes for the ESA ESM and 21 for GRACE, which both stand in complete contrast

to the results of the cattle scree test. The result for the *Guttman-Kaiser* criterion (only the modes that are higher than the average mode shall be taken) provides 22 significant modes for GRACE and 45 for ESA ESM. As the various criteria do not provide an unambiguous statement on the number of modes to be selected, a simple rule of thumb has been applied. If the difference between two adjacent singular values resp. the explained variance between two modes is low, these modes shall not be interpreted individually. This is why the first three modes of the GRACE data are chosen to be presented here. Because of consistency the first three modes of the ESA ESM have been chosen as well. Observing figure 6.14 it is remarkable that all modes, even the highest one, of the ESA ESM derived EOF modes hold a very low explained variance. This might indicate the complexity of the underlying processes. As it is mainly in the sense of comparing the different data sets and not primarily of detecting underlying physical signals, the interpretation in terms of geophysical signals will not have priority here. Much more the similarities respectively the differences between the model and the GRACE derived EOF modes will be discussed.

Figure 6.15 illustrates the first 3 EOF patterns and the corresponding PCs (Principal Components) calculated from the ESA ESM O component. The first pattern is of homogeneous positive sign and the PC shows an annual signal, having a slightly negative trend in the first three years, but a positive trend starting from 1998. This is fairly similar to the time series of the previous calculated eustatic sea-level rise and might indicate that this is the dominant signal in the Argentine Basin. The second and the the third pattern both show a more meso-scale pattern of a great number of high and low pressure fields. The poles in the EOF 2 are almost chess-pattern like arranged whereas the third EOF reveals a more spiral-shaped pattern. It will be refrained from an interpretation of the possible underlying geophysical signals here, as this can not be adequately confirmed. For the EOF analysis of the GRACE data generally the grid points over land should be masked out as only the ocean region is of interest. Certainly this leads to the appearance of the so-called *Buell pattern* (Buell, 1975) which results only because of the properties of the EOF decomposition and has no information on the spatial signal. Hence no land mask was applied during the EOF analysis to at least gain a result the ESM derived EOF modes can be compared with. Comparing the ESA ESM derived EOF mode 1 with the first EOF pattern of the GRACE data, seen in figure 6.16 (a) and the attendant PC in figure 6.16 (b), a strong similarity can be observed. The pattern in the GRACE EOF mode is though even more homogeneous than the EOF pattern derived from the simulated data. Also a strong positive trend is visible in the PC, strengthening the assumption that the eustatic sea-level rise is the predominant pattern in this region. The second EOF mode derived from GRACE data differs completely from the EOF patterns of the ESA ESM. The second EOF pattern depicts a monopole, being even strongest in the centre of the Argentine Basin. EOF 3 also strongly differs from the EOF 3 derived from the ESA ESM, revealing a dipole with a high pressure field in the south and a low pressure field near the Argentine coast. The corresponding PC shows a seasonality of 1 - 2 years. Summarizing it can be stated, that the first pattern shows great similarity, leading to the assumption that the dominant pattern is the eustatic sea-level rise. Moreover it gets obvious that the EOF pattern of the GRACE data extends over larger scale than the ESA ESM one that shows a more meso-scale to small-scale pattern, indicating that GRACE is not able to resolve any meso-scale structure yet.

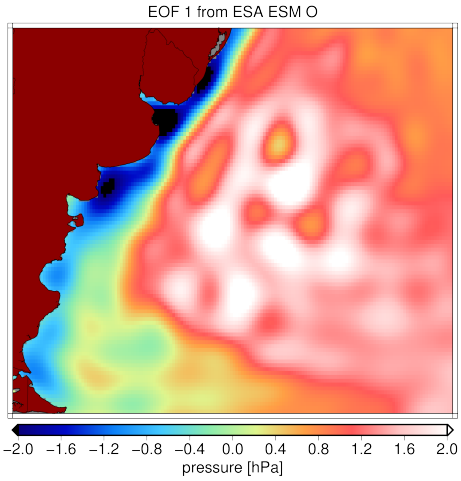

(a) EOF 1 for ESA ESM O

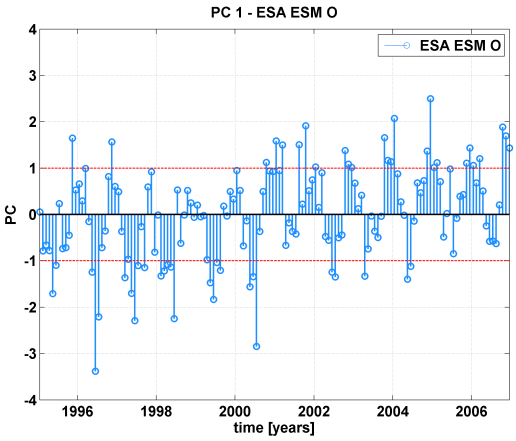

(b) PC 1 for ESA ESM O

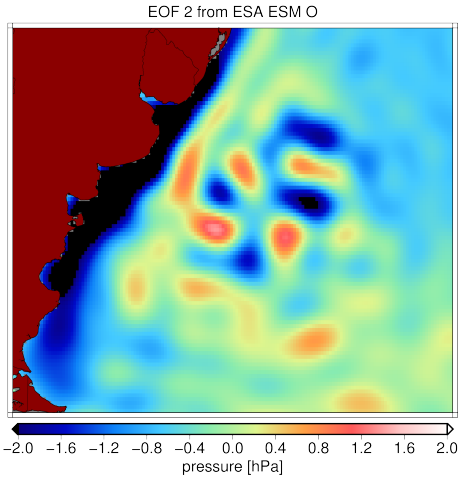

(c) EOF 2 for ESA ESM O

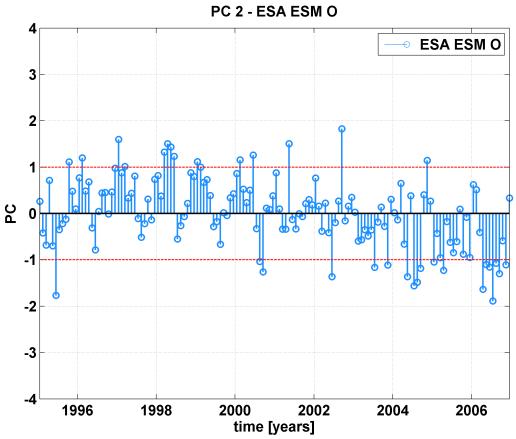

(d) PC 2 for ESA ESM O

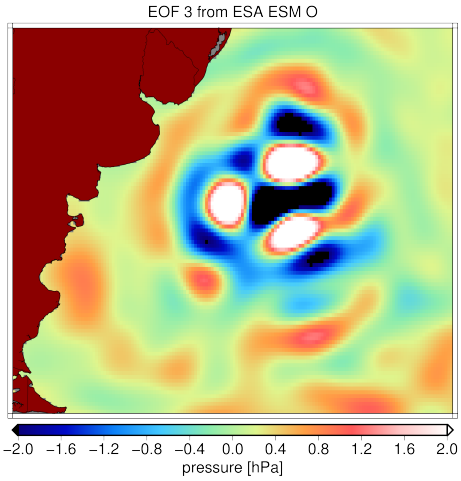

(e) EOF 3 for ESA ESM O

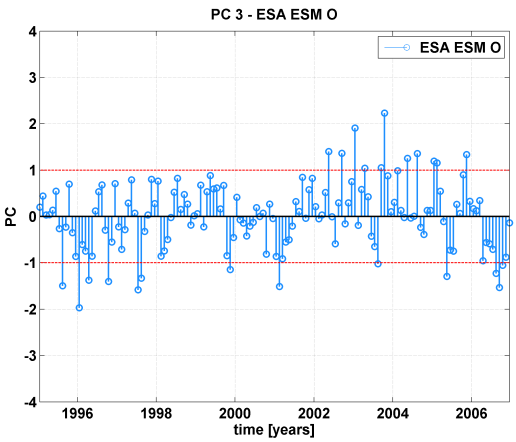

(f) PC 3 for ESA ESM O

Figure 6.15: First three EOF modes derived from the monthly averaged updated ESA ESM O component computed over 12 years (1995 - 2006)

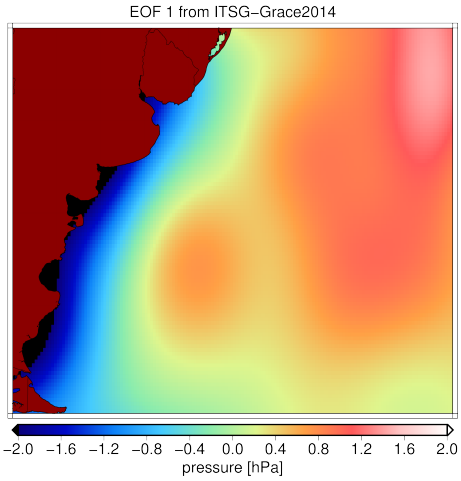

(a) EOF 1 for ITSG-Grace2014

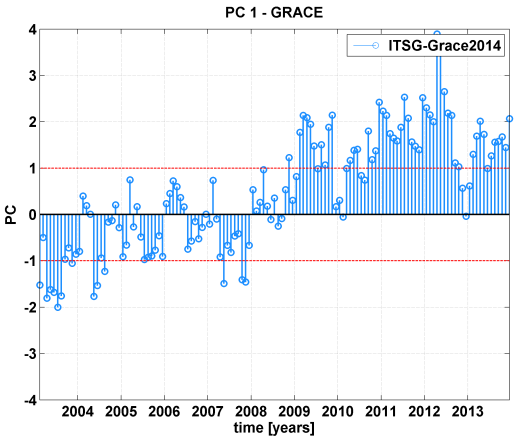

(b) PC 1 for ITSG-Grace2014

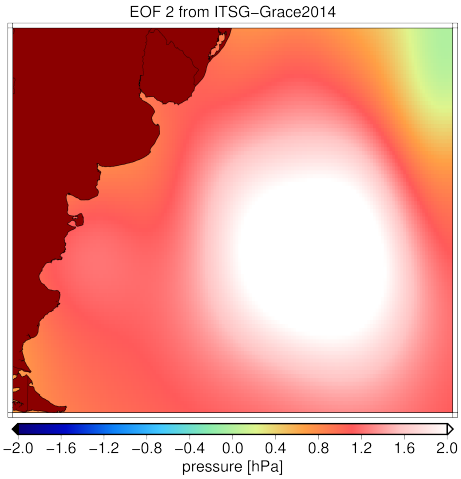

(c) EOF 2 for ITSG-Grace2014

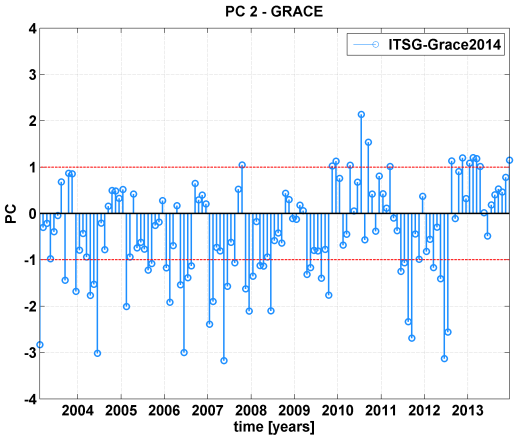

(d) PC 2 for ITSG-Grace2014

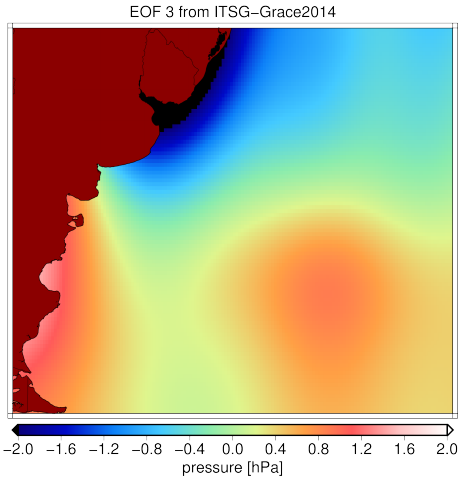

(e) EOF 3 for ITSG-Grace2014

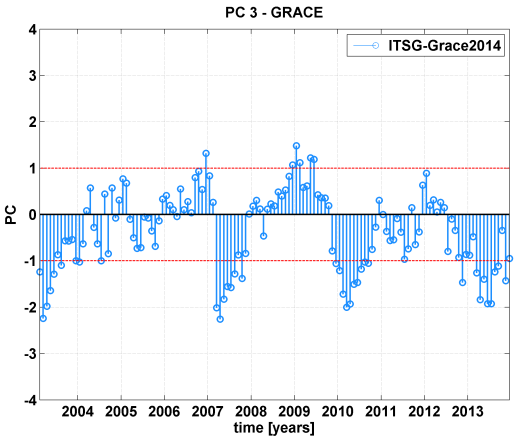

(f) PC 3 for ITSG-Grace2014

Figure 6.16: First three EOF modes derived from the ITSG-Grace2014 monthly solution computed over 11 years (2003 - 2013)

Basin-averaged RMS

Summarizing it can be stated, that no meso-scale variability in the Argentine Basin can be resolved so far by GRACE. It is not surprising that the ability of GRACE to detect meso-scale ocean processes is not satisfying, as the spatial resolution is yet too low for these variations. Even if the actual spatial resolution of GRACE would be sufficient, the mandatory use of a Gaussian filter would again blur the meso-scale variations. To give a first statement on how the spatial resolution of GRACE has to be improved in order to detect the meso-scale eddies, the mean RMS value has been calculated over the whole basin using a quadratic mean. The size of the basin and the RMS values, calculated over three years from January 2004 to December 2006, are shown in figure 6.17.

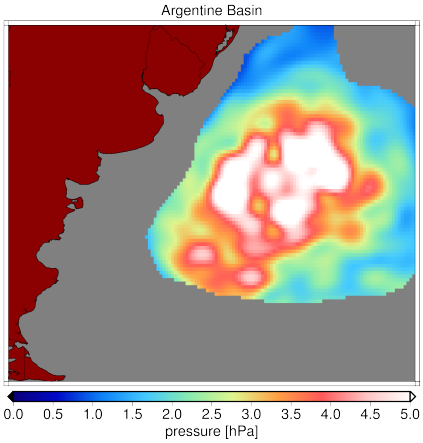

(a) OBP variations in Argentine Basin based on ESA ESM O (unfiltered)

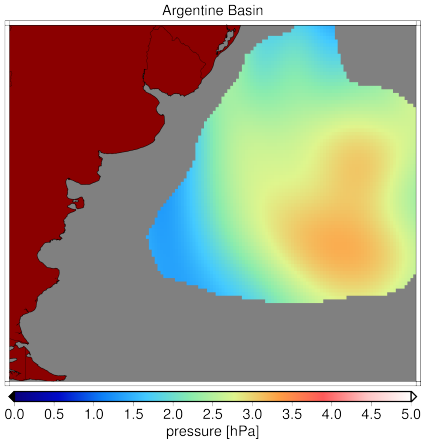

(b) OBP variations in Argentine Basin based on ITSG-Grace2014 monthly means (500 km Gaussian filtered)

Figure 6.17: RMS values in Argentine Basin used to compute basin-averaged RMS variability

Figure 6.18 depicts the mean RMS variability averaged over the whole basin in dependency on the applied Gaussian filter, comparing both the model and the gravity field solution. Additionally the formal error of the ITSG-Grace2014 gravity field solution has been propagated onto a grid to be able to calculate RMS values for the error as well. Again it has to be pointed out that the application of the different Gaussian filter radii on the depicted maximum degrees is not meaningful for all combinations. However this has been done for the sake of completeness.

From this illustration one can deduce that GRACE is definitely observing a significant signal in the Argentine Basin. Starting at the use of a Gaussian filter radius of 300 km the GRACE signal is no longer only consisting of noise. At a radius of 500 km the noise level is already conspicuously beneath the total GRACE signal, indicating the existence of a signal in this region that is far greater in signal strength than modeled through the updated ESA ESM. Having a look at figure 6.17 (b) a large-scale variability of 3.5 hPa can be detected in the basin, most likely a signal induced by the strong Zapiola Anticyclone. Filtering the ESA ESM with a 500 km Gaussian filter, a signal of only 1.25 hPa in the center of the basin remains, which is only slightly more than a third of the GRACE observed signal.

This leads to the assumption that the O component of the ESA ESM is underrating the actual signal strength of the barotropic Zapiola Anticyclone. The meso-scale variability of the updated ESA ESM however, are completely smoothed at a Gaussian radius of 200 km. As a consequence it can be stated that for the detectability of meso-scale variations in the Argentine Basin no Gaussian filter with a radius $>$ 100 km must be applied to the data. This refers to a spherical harmonic degree of 200. Furthermore, the formal GRACE error has to be reduced significantly because of the comparatively small signal content.

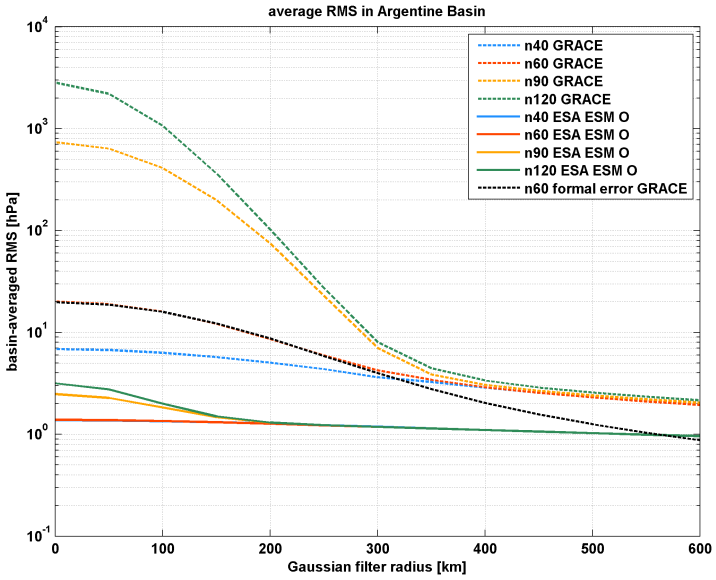

Figure 6.18: Dependency of basin-averaged RMS values on Gaussian filter radius

6.2.2 Cape Basin

For the area of the Cape Basin, lying south-west of the most southern part of South Africa, the Cape Agulhas, an observation area of 0°E to 40°E and 20°S to 45°S has been constrained. This region contains the area around the Cape Agulhas, the whole basin and within it the region with the highest rate of meso-scale eddy emergence (Dencausse et al., 2010). Basically the exact same investigations as for the Argentine Basin have been made for the Cape Basin as well, however only the results that differ from those in the Argentine Basin are represented here. Again starting with the evaluation of the RMS values, figure 6.19 and figure 6.20 show the effect of the different Gaussian filter radii on the given data sets up to a maximum degree of 120. For the ESA ESM, a significant signal of $>$ 5 hPa is visible, which is rapidly disappearing with the use of a Gaussian filter, leaving only a small fraction of the signal (2 hPa) at a filter radius of only 100 km. The results from GRACE show the same effect of the Gaussian filter as in the Argentine Basin. Figure 6.19 indicates that a Gaussian filter radius of minimum 400 km is needed to smooth the stripes. Using a 500 km radius, significant RMS values of 2.5 hPa seem to appear in the basin. Generally speaking, a minimum Gaussian filter radius of 500 km has to be used for analyzing OBP variations in ocean regions from satellite gravity data.

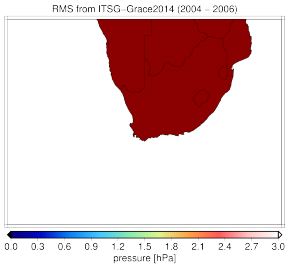

(a) 0 km Gaussian filtered

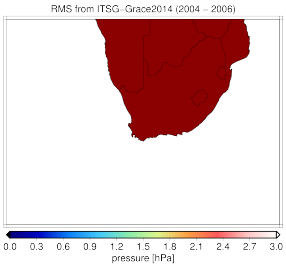

(b) 100 km Gaussian filtered

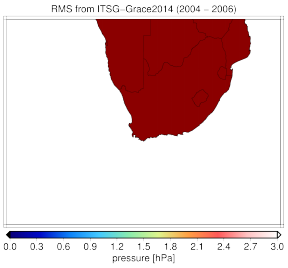

(c) 200 km Gaussian filtered

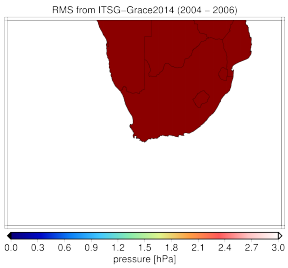

(d) 300 km Gaussian filtered

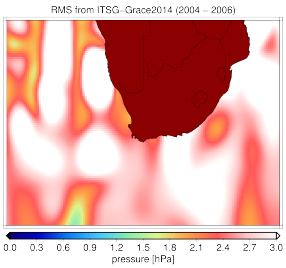

(e) 400 km Gaussian filtered

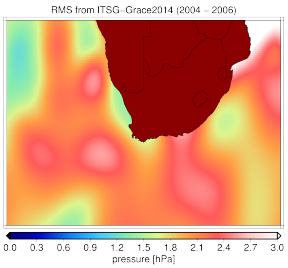

(f) 500 km Gaussian filtered

Figure 6.19: RMS values of GRACE derived OBP anomalies filtered with different Gaussian radii until d/o = 120 in the Cape Basin

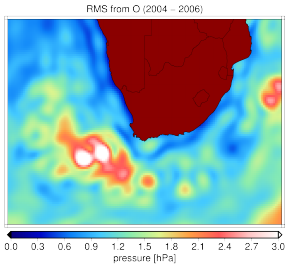

(a) 0 km Gaussian filtered

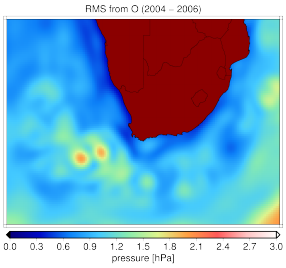

(b) 100 km Gaussian filtered

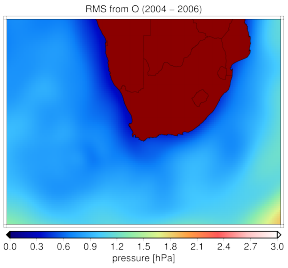

(c) 200 km Gaussian filtered

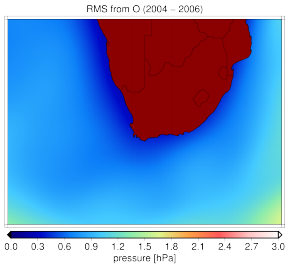

(d) 300 km Gaussian filtered

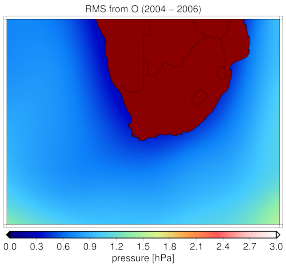

(e) 400 km Gaussian filtered

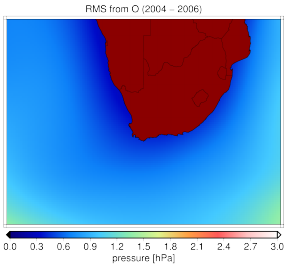

(f) 500 km Gaussian filtered

Figure 6.20: RMS values of ESA ESM derived OBP anomalies filtered with different Gaussian radii until d/o = 120 in the Cape Basin

Spatial patterns

Furthermore an EOF analysis has been carried out in order to possibly detect the sources of the previous shown OBP signals. Figure 6.21 illustrates the explained variances per mode. For the selection of the significant modes again three methods were tested, the scree test, the variance test and the Guttman-Kaiser criterion. Since all three methods resulted in completely different outcomes, the decision was to choose the modes solely on the fact that for significant modes the singular values have to differ considerably from each other. Therefore and because of consistency the first three modes were chosen to be presented and compared here.

Figure 6.22 reveals the first three EOF modes and the corresponding PCs derived from the updated ESA ESM O component. The first mode again shows good accordance between the model and the gravity field solution, probably indicating the eustatic sea-level rise. Even the EOF mode 2 reveals some similarities, especially in the according PCs, which both display a distinct annual signal. The pattern for the GRACE data shows the highest value in the south of the Cape Basin. In the same location the EOF pattern for the ESA ESM illustrates a high pressure field, though much smaller in scale. The third EOF modes do not really coincide, the Grace EOF having a dipole and the ESA ESM a meso-scale signal, again spiral-shaped like in the Argentine Basin and in the same location as before. Also the corresponding PCs do not show any significant similarities.

From the similarities between the first two EOF modes it can be assumed that the signal observed by GRACE and modeled by the ESA ESM share the same source.

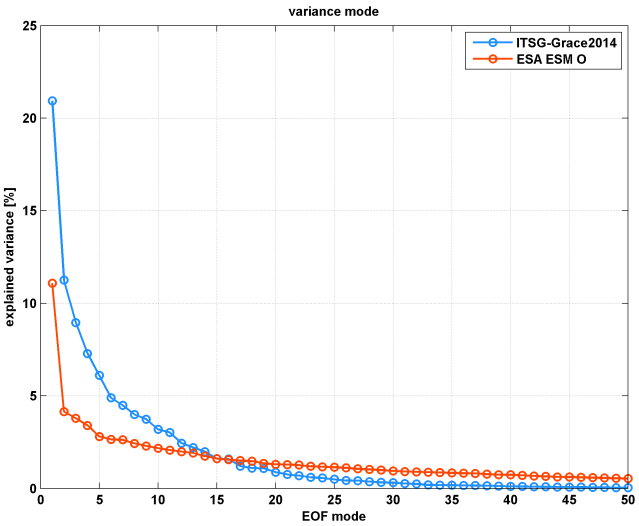

Figure 6.21: Comparison of explained variances (Cape Basin)

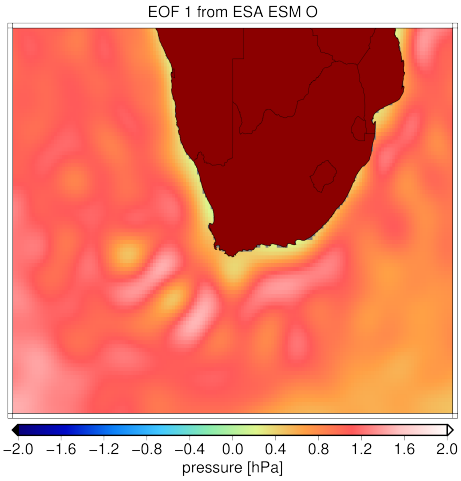

(a) EOF 1 for ESA ESM O

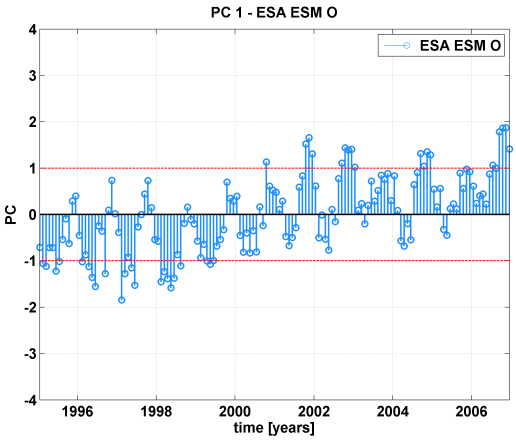

(b) PC 1 for ESA ESM O

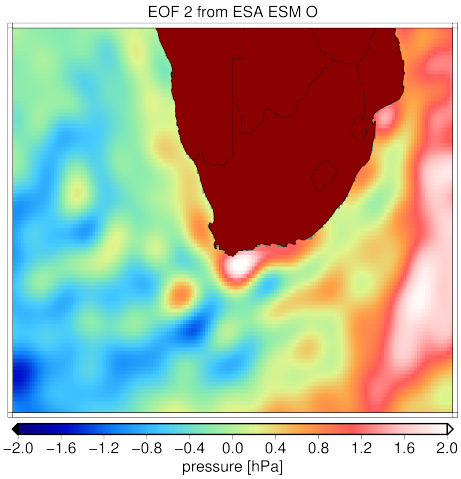

(c) EOF 2 for ESA ESM O

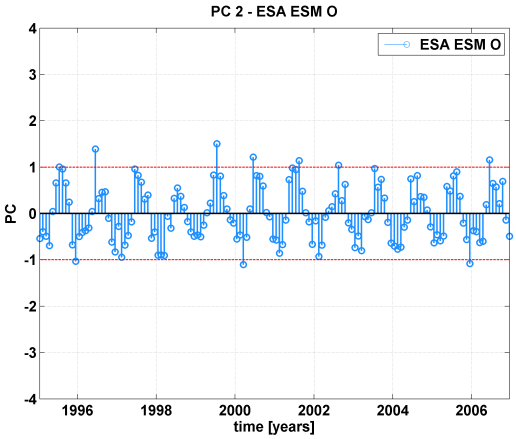

(d) PC 2 for ESA ESM O

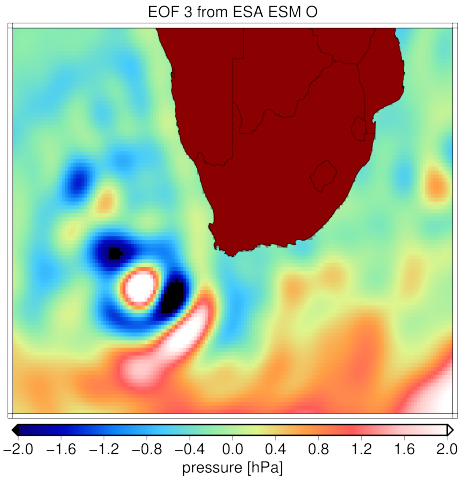

(e) EOF 3 for ESA ESM O

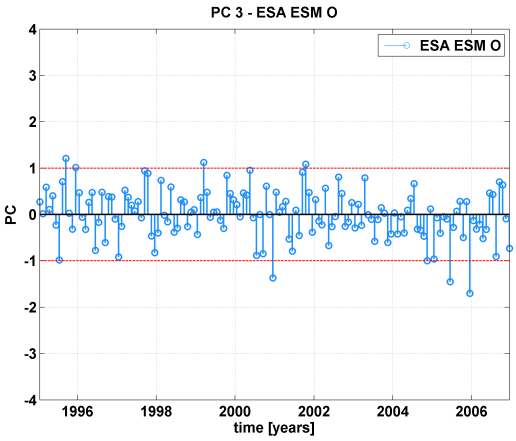

(f) PC 3 for ESA ESM O

Figure 6.22: First three EOF modes derived from the monthly averaged updated ESA ESM O component computed over 12 years (1995 - 2006)

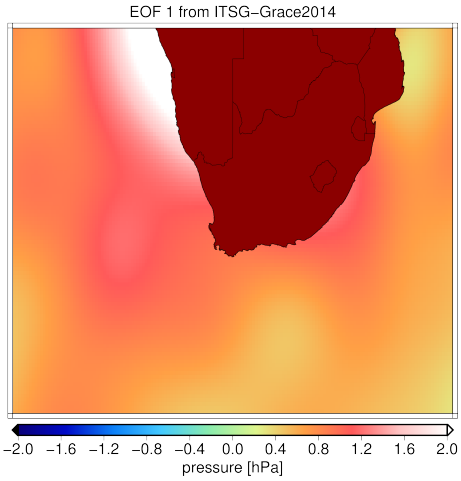

(a) EOF 1 for ITSG-Grace2014

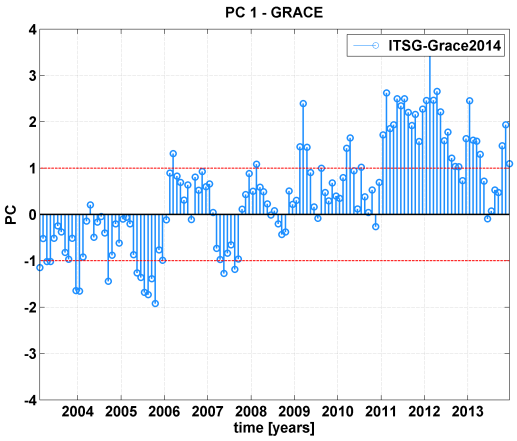

(b) PC 1 for ITSG-Grace2014

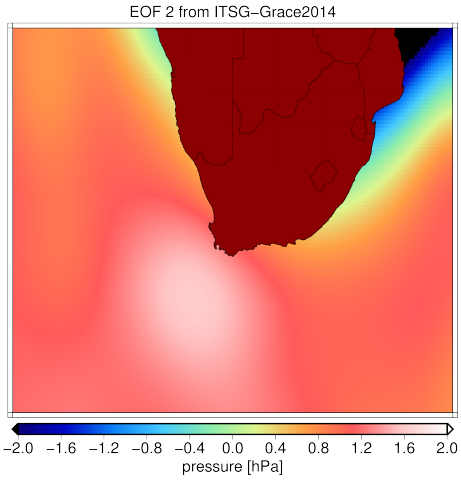

(c) EOF 2 for ITSG-Grace2014

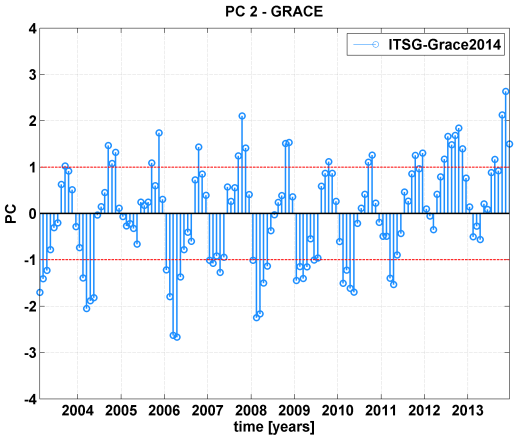

(d) PC 2 for ITSG-Grace2014

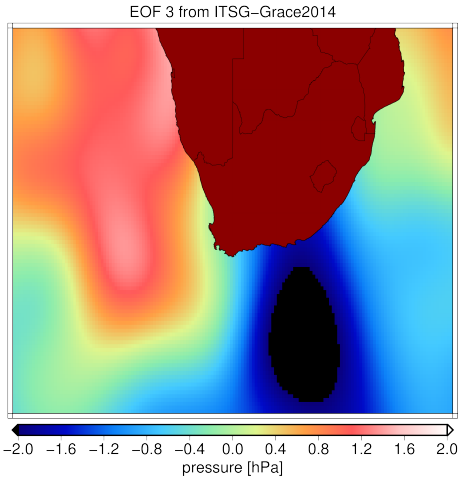

(e) EOF 3 for ITSG-Grace2014

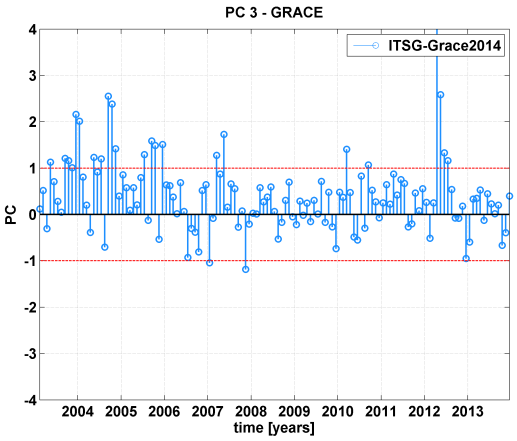

(f) PC 3 for ITSG-Grace2014

Figure 6.23: First three EOF modes derived from the monthly ITSG-Grace2014 solution computed over 11 years (2003 - 2013)

Basin-averaged RMS

In order to be able to make an assertion on the current capability of GRACE on detecting Agulhas rings, basin-averaged RMS values have been computed to compare the results in dependency on the applied Gaussian filter radius. This can be seen in figure 6.24, where the basin-averaged RMS variability for four different spherical harmonic cutoff degrees is depicted. The different cutoff degrees have been taken for the purpose of indicating that the occurrence of meso-scale variations is only modeled starting at a degree of 90. These modeled variations vanish at a use of a 200 km Gaussian filter radius, like in the Argentine Basin. The figure moreover proves the previously made statement that GRACE is observing some kind of signal when filtered with a 500 km Gaussian radius. These RMS values can not exist due to noise, as the formal GRACE error is significantly below the total GRACE signal, even for a degree of 40. Consequently it can be presumed that the updated ESA ESM is underestimating the signal in the Cape Basin.

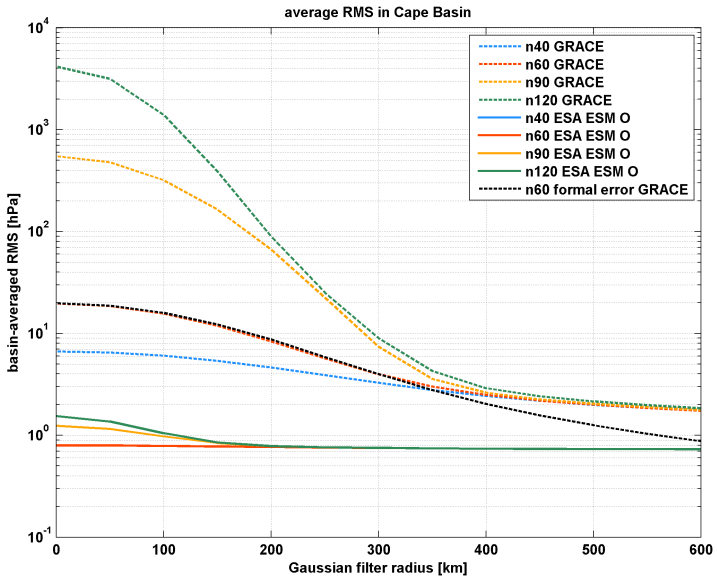

Figure 6.24: Dependency of basin-averaged RMS values on Gaussian filter radius

Let us take a closer look at the previously calculated RMS values in the Cape Basin. Figure 6.25 (a) shows the RMS values from ITSG-Grace2014 monthly solutions filtered with a 500 km Gaussian filter and 6.25 (b) the RMS values of the updated ESA ESM O component with the same filter applied. As already mentioned, because of the strong filter, no meso-scale activities in the model data are apparent. Anyway, there is still a quite strong variation visible in the RMS field of the GRACE data, indicating a strong mass induced signal in this region. Comparing the same GRACE figure with the unfiltered RMS values of the updated ESA ESM O in figure 6.25 (c), it gets obvious that the signal is present in the exact same location as the modeled meso-scale variability, though more homogeneous. This confirms the suspicion that the GRACE observed signal is the same eddy induced signal as modeled in the updated ESA ESM.

A current research work on OBP signals around the Cape Agulhas (Kuhlmann, 2013),

comparing GRACE data with a regional model as well as in-situ OBP measurements provided by the AWI (Alfred-Wegener-Institut) Bremerhaven, revealed that there is one OBP recorder measuring higher values than all the others, having a RMS value of 12.5 hPa calculated over a 2-year period. This recorder, called *AWI ANT3* is situated at 37.09°S and 12.70°W and is marked with a dot in figure 6.25 (a). This figure illustrates, that *AWI ANT3* is measuring those high values in the exact same area as the GRACE signal is present. Even the regional model set up during this research work showed RMS values of 12 hPa in the basin, which is twice as high as the maximum RMS value for the updated ESA ESM in this area. Figure 6.25 (d) pictures the maximum RMS values over a period of 3 years, reaching only around 6 hPa (please note the different scale limits in the last figure). Summarizing it can be assumed that based on the knowledge gained through the made investigations the updated ESA ESM is underrating the actual variability in the Cape Basin and GRACE might already be capable of observing a signal induced by the Agulhas rings.

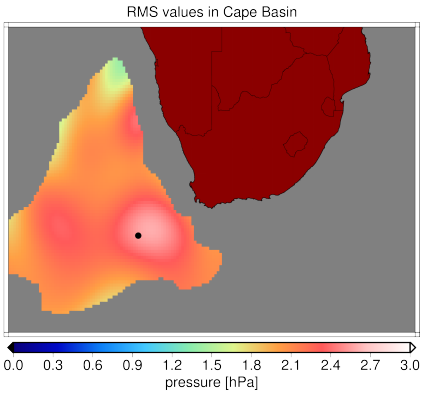

(a) OBP variations in Cape Basin based on ITSG-Grace2014 monthly means (500 km Gaussian filtered), PIES OBP recorder AWI ANT3 marked with dot

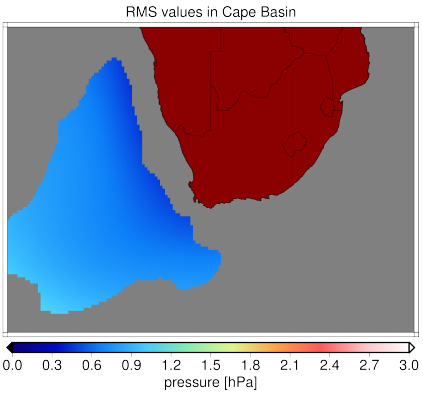

(b) OBP variations in Cape Basin based on ESA ESM O monthly means (500 km Gaussian filtered)

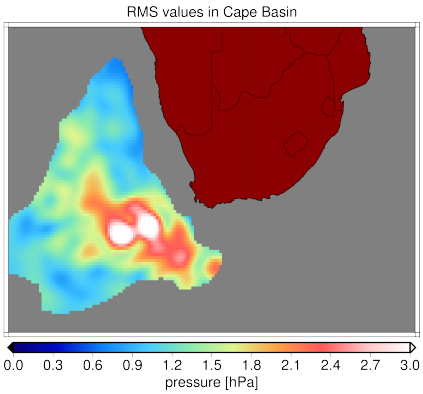

(c) OBP variations in Cape Basin based on ESA ESM O monthly means (unfiltered)

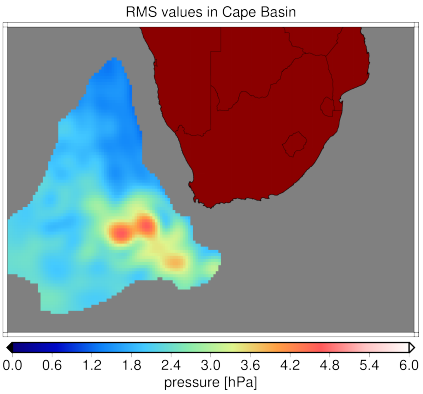

(d) OBP variations in Cape Basin based on ESA ESM O daily means (unfiltered)

Figure 6.25: Comparison of RMS values calculated over a 3-year period in the Cape Basin

6.3 Conclusion

The investigations in the two observation regions have shown that a Gaussian filter radius of 500 km is needed in both areas to detect a significant geophysical signal by reducing the systematical stripes to a minimum. The use of this relatively high filter radius is due to the low signal strength of oceanic signals, compared to continental ones. As shown in the previous chapter, the application of a Gaussian filter leads to a blurring of the signal, consequently the distinct meso-scale processes with a typical extent of 100 km, like simulated from the ESA ESM in the Argentine Basin, cannot be resolved. However, processes with a bigger spatial extent of approximately 300 km, like the cyclonic Agulhas rings in the Cape Basin, already leave a substantive footprint in the low degree coefficients of GRACE. Moreover it has been pointed out, that the modeled OBP variations in the ESA ESM might underestimate these rings. To make a general statement on the demands of future GRACE missions to resolve meso-scale eddy activity in the ocean, the degree and error degree variances of the ITSG-Grace2014 gravityfield solution as well as the ESA ESM have been computed and are illustrated in figure 6.26. The continuous purple line marks the degree amplitudes of the static ITSG-Grace2014 solution, the dashed purple ones the error degree amplitudes of various monthly solutions. This was chosen in order to show that the accuracy of the results depends on the months used in the evaluation process. The continuous blue line presents the degree amplitudes of the ESA ESM.

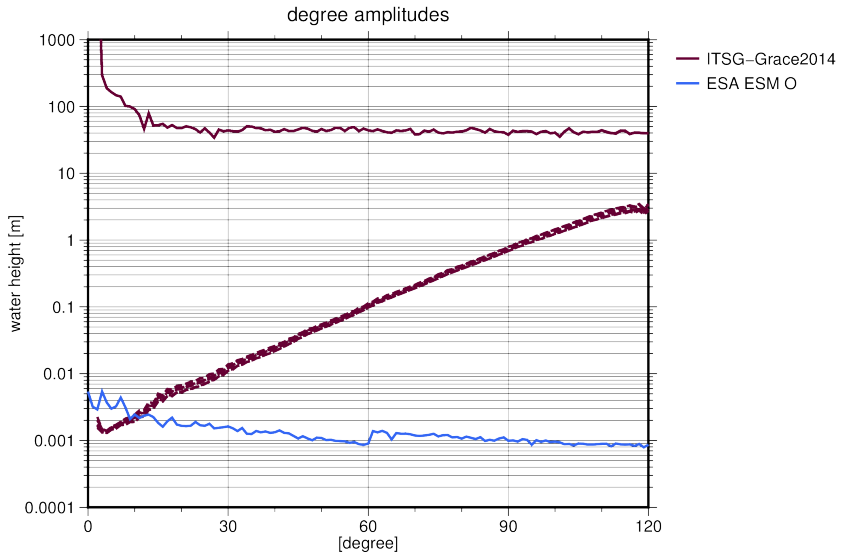

Figure 6.26: Degree amplitudes from GRACE monthly solutions (04-2004, 04-2005, 04-2006, 04-2007, 04-2008 and 04-2009) and ESA ESM O

Looking at figure 6.26 one could draw the conclusion that GRACE is only able to resolve oceanic processes up to a maximum degree of 10, as the formal errors are intersecting the curve of the ESA ESM degree amplitudes at this certain degree. The figure is however misleading, as the properties of degree variances being calculated globally distort the actual oceanic signal content of the ESA ESM by including the land masses (which do not contain any signal at all for the ocean component) in the degree variance computation. Consequently the actual signal content is higher in reality than demonstrated here, proba-

bly by a factor 10. The intersection between the formal GRACE error and the model would subsequently be around degree 30, which is more realistic. However, one has to keep in mind that this is just a global assumption, hence regional divergences can definitely exist. This is one of the difficulties in providing a clear statement on the necessary improvement of the GRACE accuracy.

Furthermore the widespread definition of meso-scale, varying between $<$ 100 km to 300 km, makes it hard to postulate a distinct factor for an upgrade accuracy. Referring to the figures 6.18 and 6.24 it can definitely be said that a maximum Gaussian filter of 100 km must be used to still observe meso-scale variations like they are modeled in the ESA ESM. This gives rise to the assumption that at least a gravity field solution of maximum degree 200 is needed. However, as mentioned before, signals induced by processes of 200 - 300 km in diameter are already visible at a degree of 40 in the GRACE solutions, probably also because of the transient nature of the Agulhas rings. To better resolve their structure, at least a degree of 90-100 should be sufficient. On the assumption that the updated ESA ESM is underrating the actual signal strength of the Agulhas rings and the resulting fact that the variations in the Cape Basin might be around 10 hPa (which corresponds to 10 cm EWH) or higher, a factor of only one decimal power in improvement of the formal GRACE error is needed. This, however is only valid for the large cyclonic Agulhas rings.

In the Argentine Basin, the meso-scale eddies are smaller in contrast to the Agulhas rings, having only diameters of 100 km or less. Anyway, several of those eddies can exist at the same time, so that the eddy induced signal is far larger in scale. Furthermore a second very strong signal is present in the basin, partly overlapping with the region of meso-scale activity. A separation of those signals is not possible at the moment, hence it can not be said for sure that the current observed signal in the basin is barely due to the Zapiola Anticyclone and not due to meso-scale eddy activity. To resolve those single eddies and separate them from the Zapiola Anticyclone, a maximum degree of 200 seems to be a minimum requirement as any applied filter with a filter radius $>$ 100 km will blur the signal too much and make a signal separation impossible. An estimation of a resulting improvement factor is difficult in this case, but is definitely one to two decimal power more than for the Agulhas region. This assumption is also valid for the smaller Agulhas rings. Moreover, some physical processes are currently disregarded in the GRACE AOD1B RL05 respectively in the OMCT as the grid resolution is too low to accurately resolve them. (Dobslaw et al., 2015) showed that the contribution of omitting these physical processes does not have a very high effect on the total error de-aliasing budget for now. However, the use of a higher-resolution model in the de-aliasing process would also affect the actual accuracy of GRACE and hence also the possibility to detect these meso-scale variability. An assessment on how much the accuracy would improve through that can however not be given here. Consequently it can be stated, that the needed requirements for detecting meso-scale ocean variations strongly depend on the region as well as on the nature of the present meso-scale processes. The given assumptions were furthermore made on the basis of a comparison with the ESA ESM, which might also currently underestimate some processes. Therefore it might occur that an even lower factor of improvement is sufficient to detect meso-scale variability in one of these basins. All the mentioned circumstances lead to the conclusion that no globally valid statement on the accuracy requirements for future satellite gravity missions to detect meso-scale variability can be made.

7 Outlook

A more concrete statement on the required improvement of the accuracy of future satellite gravity missions might be given when the data of the GRACE-FO mission is ready to use. The successor mission of GRACE-1 is planned to be launched in 2017 and its main aim is to continue the GRACE time series. This mission, however, will not exceed the level of accuracy of the GRACE-1 mission, as it uses the same measurement principle and microwave ranging system[1]. The chances to detect meso-scale ocean variability will be greater in future satellite gravity missions, following the GRACE-FO mission. An innovative orbit configuration, called Bender Configuration (Bender et al., 2008), is in discussion for a new satellite gravity mission. This configuration, composed of two satellite pairs on two different orbits, shall gain a reduction of the typical GRACE stripes which would be of great advantage for the detection of meso-scale eddies as the use of a Gaussian filter might not be mandatory and hence less high-frequency signal content would get lost.

Beside the reduction of the stripes, some effort has to be put into the improvement of the background models used during the processing of the GRACE gravity field solutions. The errors of these models play a major role in the total error budget and are hence a big issue in the improved accuracy to be achieved. Through the combination of innovative satellite constellations, improved sensors and upgraded background models, a detection of meso-scale ocean variability should be possible in most ocean regions for satellite gravity missions following the planned GRACE-FO.

[1] http://gracefo.jpl.nasa.gov/mission/, accessed 2015/08

List of Figures

List of Tables

List of Abbreviations

GRACE	Gravity Recovery and Climate Experiment
ESA ESM	European Space Agency Earth System Model
OBP	Ocean Bottom Pressure
NASA	National Aeronautics and Space Administration
DLR	Deutsches Zentrum für Luft- und Raumfahrt
SST-ll	Satellite-to-Satellite Tracking in low-low configuration
CHAMP	Challenging Mini Satellite Payload
GRACE-FO	GRACE Follow On
CSR	Texas Center for Space Research
GFZ	GeoForschungsZentrum Potsdam
JPL	Jet Propulsion Laboratory
PGR	Post Glacial Rebound
GIA	Glacial Isostatic Adjustment
AOD1B RL05	Atmosphere and Ocean De-aliasing Level-1B Release 05
OMCT	Ocean Model for Circulation and Tides
CM	Center of Mass
CF	Center of Figure
RMS	Root Mean Square
EOF	Empirical Orthogonal Function
UTC	Universal Time Coordinated
IB	Inverse Barometer
MPIOM	Max-Planck-Institute for Meteorology Ocean Model
HOPE	Hamburg Ocean Primitive Equation
EWH	Equivalent Water Height
PODAAC	Physical Oceanography Distributed Active Archive Center
ACC	Antarctic Circumpolar Current
AWI	Alfred-Wegener-Institut

Bibliography

Bender, P. L., Wiese, D. N., and Nerem, R. S. A possible dual-grace mission with 90 degree and 63 degree inclination orbits. In *in Proceedings, 3rd International Symposium on Formation Flying, Missions and Technologies. European Space Agency Symposium Proceedings, ESA SP-654.*, Noordwijk, The Netherlands, 2008. ESA, ESA. JILA Pub. 8161.

Bryan, F., Wahr, J., and Molenaar, M. Time-variability of the Earth´s gravity field: Hydrological and oceanic effects and their possible detection using GRACE. 103:205–229, 1998.

Buell, C. E. *The topography of empirical orthogonal functions.* Fourth Conf. on Probability and Statistics in Atmospheric Sciences, Tallahassee, FL, Amer. Meteor. Soc., 188–193, 1975.

Cattell, R. B. The scree test for the number of factors. *Multivariate Behavioral Research 1, 245–276*, 1966.

Church, J., Clark, P., Cazenave, a., Gregory, J., Jevrejeva, S., Levermann, a., Merrifield, M., Milne, G., Nerem, R., Nunn, P., a.J. Payne, Pfeffer, W., Stammer, D., and a.S. Unnikrishnan. Sea level change. *Climate Change 2013: The Physical Science Basis. Contribution of Working Group I to the Fifth Assessment Report of the Intergovernmental Panel on Climate Change*, pages 1137–1216, 2013.

CIESM. Strategies for understanding mesoscale processes. *CIESM Workshop Monographs n°27, 132 pages, Monaco*, 2005. URL `www.ciesm.org/online/monographs/villefranche05.pdf`.

Colling, A., Brown, E., Park, D., Phillips, J., Rothery, D. R., and Wright, J. *Ocean Circulation.* The Open University, 2001.

de Miranda, A., Barnier, B., and Dewar, W. K. On the dynamics of the zapiola anticyclone. *Jounral of Geophysical Research Vol. 104, No. C9, Pages 137-149*, 1999.

Dencausse, G., Arhan, M., and Speich, S. Routes of Agulhas rings in the southeastern Cape Basin. *Deep-Sea Research Part I: Oceanographic Research Papers*, 57(11):1406–1421, 2010. ISSN 09670637. doi: 10.1016/j.dsr.2010.07.008.

Dobslaw, H., Wolf, I. B., Forootan, E., Klemann, V., and Kusche, J. *Updating ESA ' s Earth System Model for Gravity Mission Simulation Studies 3 . A Realistically Perturbed Non-Tidal Atmosphere and Ocean De-Aliasing Model.* 2015. ISBN 4000109421. doi: 10.2312/GFZ.b103-14091.

Dobslaw, H. *Modellierung der allgemeinen ozeanischen Dynamik zur Korrektur und Interpretation von Satellitendaten.* PhD thesis, Technische Universität Dresden, 2007.

Dobslaw, H., Bergmann-Wolf, I., Dill, R., Forootan, E., Klemann, V., Kusche, J., and Sasgen, I. Updating ESA's Earth System Model for Gravity Mission Simulation Studies: 1. Model Description and Validation. *Scientific Technical Report 14/07, GFZ German Research Centre for Geosciences*, 2014. doi: 10.2312/GFZ.b103-14079.

Dommenget, D. and Latif, M. A cautionary note on the interpretation of EOFs. *Journal of Climate*, 15(2):216–225, 2002.

Drakos, N. Ocean models. website, 1994. URL `http://www.phy.ornl.gov/csep/om/om.html`. Computer Based Learning Unit, University of Leeds.

Drijfhout, S., Heinze, C., Latif, M., and Maier-Reimer, E. Mean circulation and internal variability in an ocean primitive equation model. *J. Phys. Oceanogr., 26, 559-580*, 1996.

Flechtner, F. Gravity Recovery and Climate Experiment AOD1B Product Description Document. *AOD1b Product Description Document*, 750:1–33, 2007.

Gruber, T., Bamber, J., Bierkens, M., Dobslaw, H., Murböck, M., Thomas, M., Beek, L. v., Dam, T. v., Vermeersen, L., and Visser, P. *Earth System Science Data, volume 3, pp. 19 - 35*, 2011.

Gruber, T. and Flechtner, F. Vereinfachte Darstellung der GRACE Datenanalyse. *System*, pages 1–5, 2007. URL `http://www.dgfi.badw.de/typo3_mt/fileadmin/vortraegeGummersbach/gruber_flechtner_grace_processing.pdf`.

Hannachi, A. A primer for EOF analysis of climate data. *Reading: University of Reading*, pages 1–33, 2004. URL `http://www.o3d.org/eas-6490/lectures/EOFs/eofprimer.pdf`.

Heiskanen, W. A. and Moritz, H. *Physical Geodesy.* W.H.Freeman & Co Ltd, 1967.

Horwath, M. *Zur Ermittlung geophysikalischer Massensignale mit Schwerefeldmissionen: Eine Analyse des gegenwärtigen Standes am Beispiel der Antarktis.* PhD thesis, Technische Universität Dresden, 2007.

Hughes, C. W., Stepanov, V. N., Fu, L. L., Barnier, B., and Hargreaves, G. W. Three forms of variability in Argentine Basin ocean bottom pressure. *Journal of Geophysical Research: Oceans*, 112(1):1–17, 2007. ISSN 21699291. doi: 10.1029/2006JC003679.

Jungclaus, J. H., Fischer, N., Haak, H., Lohmann, K., Marotzke, J., Matei, D., Mikolajewicz, U., Notz, D., and Von Storch, J. S. Characteristics of the ocean simulations in the Max Planck Institute Ocean Model (MPIOM) the ocean component of the MPI-Earth system model. *Journal of Advances in Modeling Earth Systems*, 5(2):422–446, 2013. ISSN 19422466. doi: 10.1002/jame.20023.

Klemann, V., Martinec, Z., and Ivins, E. R. Glacial isostasy and plate motion. *Journal of Geodynamics*, 46(3-5):95–103, 2008. ISSN 02643707. doi: 10.1016/j.jog.2008.04.005.

Kuhlmann, J. *Simulated And Observed Sea Level And Ocean Mass Variations*. PhD thesis, Freie Universität Berlin, 2013.

Kurtenbach, E. *Entwicklung eines Kalman-Filters zur Bestimmung kurzzeitiger Variationen des Erdschwerefeldes aus Daten der Satellitenmission GRACE*. PhD thesis, Institut für Geodäsie und Geoinformation Bonn, 2011.

Lehahn, Y., D'Ovidio, F., Lévy, M., Amitai, Y., and Heifetz, E. Long range transport of a quasi isolated chlorophyll patch by an Agulhas ring. *Geophysical Research Letters*, 38 (16):1–6, 2011. ISSN 00948276. doi: 10.1029/2011GL048588.

Mayer-Gürr, T., Zehentner, N., Klinger, B., and Kvas, A. Itsg-grace2014 - a new grace gravity field release computed in graz. *GRACE Science Team Meeting (GSTM), Potsdam*, 2014.

Monahan, A. H., Fyfe, J. C., Ambaum, M. H. P., Stephenson, D. B., and North, G. R. Empirical Orthogonal Functions: The Medium is the Message. 2009. ISSN 0894-8755. doi: 10.1175/2009jcli3062.1. URL `http://dx.doi.org/10.1175/2009jcli3062.1`.

Paulson, Z. S., A. and Wahr, J. Inference of mantle viscosity from grace and relative sea level data. 2007. doi: 10.1111/j.1365-246X.2007.03556.x.

Peltier, W. R. Closure of the budget of global sea level rise over the GRACE era: the importance and magnitudes of the required corrections for global glacial isostatic adjustment. *Quaternary Science Reviews*, 28(17-18):1658–1674, 2009. ISSN 02773791. doi: 10.1016/j.quascirev.2009.04.004. URL `http://dx.doi.org/10.1016/j.quascirev.2009.04.004`.

Peters, T. *Modellierung zeitlicher Schwerevariationen und ihre Erfassung mit Methoden der Satellitengravimetrie*. PhD thesis, Technische Universität München, 2007.

Quinn, K. J. and Ponte, R. M. Uncertainty in ocean mass trends from grace. *Geophysical Journal International, 181: 762–768*, 2010. doi: 10.1111/j.1365-246X.2010.04508.x.

Saunders, P. and King, B. Bottom currents derived from a shipborne adcp on the woce cruise all in the south atlantic. *Jounral of Physical Oceanography, 25, 329-347*, 1995.

ScienceDaily. Ocean currents off south africa influence gulf stream. *Leibnitz Marine Institute*, 2008. URL `www.sciencedaily.com/releases/2008/11/081126133539.htm`.

Simmons, A. J., Wallace, J. M., and Branstator, G. W. Barotropic wave propagation and instability, and atmospheric teleconnection patterns. *Journal of Atmospheric Sciences, vol. 40, Issue 6, pp.1363-1392*, 1983.

Swenson, S. and Wahr, J. Post-processing removal of correlated errors in GRACE data. *Geophysical Research Letters*, 33(8):1–4, 2006. ISSN 00948276. doi: 10.1029/2005GL025285.

Swenson, S., Chambers, D., and Wahr, J. Estimating geocenter variations from a combination of GRACE and ocean model output. *Journal of Geophysical Research: Solid Earth*, 113(8):1–12, 2008. ISSN 21699356. doi: 10.1029/2007JB005338.

Thomas, M. and Dobslaw, H. On the impact of baroclinic ocean dynamics on the Earth's gravity field. *Proc. Joint CHAMP/GRACE Science Team Meeting*, page 6, 2004. URL `http://www-app2.gfz-potsdam.de/pb1/JCG/Thomas_and_Dobslaw_jcg.pdf`.

von Storch, H. and Zwiers, F. W. *Statistical Analysis in Climate Research*. Cambridge University Press, Cambridge, x+484pp, 1999.

Wahr, J. M. A method of inferring changes in deep ocean currents from satellite measurements of time-variable gravity. *Journal of Geophysical Research*, 107(C12):1–17, 2002. ISSN 0148-0227. doi: 10.1029/2001JC001274.

Wolff, J., Maier-Reimer, E., and Legutke, S. The hamburg ocean primitive equation model hope. *Technical Report 13, Deutsches Klimarechenzentrum, Hamburg, Germany, 103pp*, 1997.

Wunsch, C. and Stammer, D. Atmospheric loading and the oceanic inverted barometer effect. *Reviews of Geophysics, 35, pages 79-107*, 1997.